Regulation of sphingolipid synthesis by the C2H2 zinc finger transcription factor Com2 through ubiquitin-proteasome mediated degradation pathway

Kosei Matsumoto[1†], Ayane Nagai[1†], Nao Komatsu[1†], Yuko Ishino[1†], Rina Shirai[1†], Toshiya Ueno[1], Mio Masaki[1], Ken-taro Sakata[1], Motohiro Tani[2], Tatsuya Maeda[3], Naotaka Tanaka[1], and Mitsuaki Tabuchi[1*]

[1] Department of Applied Biological Science, Faculty of Agriculture, Kagawa University, Miki-cho, Kagawa, 761-0795, Japan

[2] Faculty of Applied Biological Science, Gifu University, Yanagido 1-1, Gifu 501-1193, Japan

[3] Department of Biology, Hamamatsu University School of Medicine, Handayama, Chuo-ku, Hamamatsu, Shizuoka, 431-3192, Japan

[*] For correspondence: tabuchi.mitsuaki@kagawa-u.ac.jp

[†] These authors contributed equally to this work.

Running Title: Transcriptional regulation of sphingolipid metabolism in budding yeast.

Keywords: lipid metabolism, sphingolipid, transcription factor, TORC2, *Saccharomyces cerevisiae*, ubiquitin-proteasome system

Abstract

Membrane lipid synthesis is globally coordinated by a limited set of master transcription factors that regulate broad gene networks encoding lipid-metabolic enzymes and their regulators. Here, we identify the C2H2 zinc-finger transcription factor Com2 as a regulator of sphingolipid homeostasis in *Saccharomyces cerevisiae* that promotes transcription of downstream targets, including the protein kinase Ypk1, a key activator of sphingolipid synthesis. Com2 protein abundance increased upon treatment with myriocin, an inhibitor of sphingolipid synthesis, but rapidly decreased after addition of phytosphingosine (PHS), a precursor of complex sphingolipids; this decrease was blocked by proteasome inhibitors. These results suggest that Com2 is regulated in a sphingolipid-dependent manner through proteasome-mediated degradation. Moreover, a Com2 mutant in which lysine residues putatively involved in ubiquitination were replaced with arginine exhibited attenuated PHS-dependent degradation and elevated phosphorylation. Likewise, a mutant in which putative phosphorylation sites were replaced with alanine showed reduced PHS-dependent degradation. Together, these findings indicate that Com2 undergoes phosphorylation-dependent degradation via the ubiquitin–proteasome system in response to sphingolipid levels.

Introduction

Cell membranes are composed of lipid bilayers, which consist of three major types of membrane lipids: glycerophospholipids, sphingolipids, and sterols (mainly cholesterol in mammals and ergosterol in yeasts) (van Meer et al., 2008). The synthesis of lipid bilayers during membrane formation involves the coordinated assembly of multiple lipid species, which requires the coordination of different levels, including lipid synthesis, uptake, metabolism, and subcellular distribution (Breslow and Weissman, 2010; Nohturfft and Zhang, 2009). This homeostasis is important for the maintenance of cellular and tissue functions, and its dysfunction in humans can lead to numerous diseases, such as cancer or type-2 diabetes (Harayama and Riezman, 2018). The principal instruments for the global control of lipid metabolism are regulated by master transcriptional regulators, which target genes encoding metabolic enzymes and/or their regulators working in specific metabolic pathways (Nohturfft and Zhang, 2009).

For example, in yeast, the transcription factors Ino2/Ino4 function in the expression of several glycerophospholipid synthases (Kwiatek et al., 2020). Under logarithmic growth or inositol-depleted conditions, the repressor Opi1 is bound to the endoplasmic reticulum (ER) membrane in a phosphatidic acid (PA)-dependent manner, and Ino2/Ino4 promote transcription. However, in steady-state or inositol-rich conditions, the decrease in PA on the ER membrane causes Opi1 to translocate to the nucleus, thereby inhibiting Ino2/Ino4-dependent transcription and repressing glycerophospholipid synthesis (Ambroziak and Henry, 1994; Loewen, 2003; Loewen et al., 2004; White et al., 1991). In the cholesterol metabolism of animal cells, the membrane-bound transcription factors, SREBPs, are synthesized as inactive precursors that are anchored in the membrane of the ER under sterol-rich conditions (Hua et al., 1996). SREBPs are translocated to the Golgi apparatus in a COPII vesicle-dependent manner (Nohturfft et al., 2000, 1999, 1998), where it is sequentially cleaved by Site-1 and Site-2 proteases, detached from the membrane (Rawson et al., 1997; Sakai et al., 1998, 1996; Wang et al., 1994), and translocated to the nucleus, thus promoting the expression of genes involved in cholesterol metabolism, such as HMG CoA reductase, the rate-limiting enzyme in cholesterol metabolism (Goldstein et al., 2006; Nohturfft and

Zhang, 2009). Thus, in glycerophospholipid and sterol metabolism, it is well known that the synthesis of these lipids is coordinately regulated by master transcriptional regulators, in both yeast and mammals. However, master transcriptional regulators of sphingolipid metabolism remain elusive (Breslow and Weissman, 2010).

Sphingolipids and their metabolites play key cellular roles as both structural components of membranes and as signaling molecules that mediate responses to physiological cues (Breslow and Weissman, 2010). Recent studies using budding yeast, *Saccharomyces cerevisiae*, as a model system have improved our understanding of metabolic enzymes and how these enzymes are regulated to ensure sphingolipid homeostasis (Breslow et al., 2010; Breslow and Weissman, 2010). The regulation of sphingolipid metabolism by the target of rapamycin (TOR) complex 2 (TORC2)-Ypk1 pathway has been studied in detail in yeast (Berchtold et al., 2012; Eltschinger and Loewith, 2016; Niles et al., 2012; Tabuchi et al., 2006). As a regulatory mechanism of sphingolipid biosynthesis, TORC2, in concert with Slm1/2, which was identified as a synthetic lethal gene along with *MSS4* encoding a phosphatidylinositol 4-phosphate 5-kinase (Audhya et al., 2004; Tabuchi et al., 2006), phosphorylates Ypk1 upon depletion of complex sphingolipids at the plasma membrane (Berchtold et al., 2012; Niles et al., 2012). Phosphorylated Ypk1 further phosphorylates Orm1/2, which negatively regulates serine palmitoyl transferase (SPT) (Breslow et al., 2010; Gururaj et al., 2013; Roelants et al., 2011), which is the first step in sphingolipid metabolism. Thereafter, the phosphorylation of Orm1/2 through Ypk1 results in an increase in SPT activity. The TORC2-Ypk1 signal has also been reported to activate ceramide synthase by phosphorylating the N-terminal sites of the ceramide synthase catalytic subunits, Lag1/Lac1 (Muir et al., 2014). Together, TORC2-Ypk1-dependent signaling simultaneously upregulates the two most important steps in the sphingolipid biosynthetic pathway.

While investigating how reduced ceramide synthesis affects the TORC2-Ypk1 pathway using the ceramide synthase regulatory subunit mutant *lip1-1*, we found that *lip1-1* is hypersensitive to myriocin (Myr), a specific inhibitor of SPT (Fig. 1A) (Ishino et al., 2022).

To identify novel regulators of sphingolipid metabolism, we performed a multicopy suppressor screen for genes that alleviate the Myr sensitivity of *lip1-1* cells. This approach led to the identification of Com2, a C2H2-type zinc finger transcription factor that had not previously been linked to sphingolipid metabolism. Further analyses revealed that Myr-induced sphingolipid depletion resulted in increased Com2 expression, accompanied by elevated Ypk1 expression and enhanced TORC2-dependent phosphorylation of Ypk1. In *com2*Δ cells, both the Myr-induced upregulation of Ypk1 and its activation by TORC2 were markedly reduced. Moreover, deletion of the Com2-binding site (CBS) in the *YPK1* promoter abolished these inductions, indicating that Ypk1 upregulation in response to sphingolipid depletion depends on Com2 and the CBS element in the *YPK1* promoter. We further found that Com2 is rapidly degraded via the ubiquitin-proteasome system (UPS) upon addition of exogenous sphingolipid precursor, demonstrating that Com2 abundance is primarily controlled through UPS-dependent proteolysis in a sphingolipid-dependent manner.

Collectively, these findings suggest that Com2 acts as a master transcription factor that senses intracellular sphingolipid levels, regulates CBS-dependent target genes such as *YPK1*, and is itself controlled by sphingolipid-dependent degradation via the ubiquitin–proteasome system.

Results

A screen for novel regulatory factors involved in sphingolipid metabolism

We previously generated and characterized a $P_{tet\text{-}off}$-*lip1-1* (*lip1-1*) strain in which ceramide synthesis decreased in the presence of doxycycline (Dox) (Ishino et al., 2022). Dox-treated *lip1-1* cells are hypersensitive to myriocin (Myr), an inhibitor of serine palmitoyltransferase (SPT), the first step in sphingolipid biosynthesis (Figure 1A), presumably due to the synthetic effect of the Dox-dependent decrease in ceramide synthesis and inhibition of SPT. We hypothesized that overexpressing a protein involved in sphingolipid biosynthesis would confer Myr resistance to *lip1-1* cells. To identify novel regulatory factors, we transformed *lip1-1* cells with a multi-copy genomic library and selected transformants that grew on Myr-containing media (Figure 1B). Sequencing 27 Myr-resistant plasmids revealed 12 gene groups (*MLM* genes: *M*ulti-copy suppressor for *L*ip1-1 *M*yr-sensitive phenotype, Figure1—figure supplement 1, Table 1). Among these, the *YPK1* (*MLM5*), which encodes for a protein kinase downstream of the TORC2 signaling pathway, which is known to be involved in the regulation of sphingolipid metabolism (Figure 1C), was identified, thus validating that genes involved in the regulation of sphingolipid metabolism can be obtained employing this screening. Besides the *LIP1* (*MLM1*), the *COM2* (*MLM2*), which encodes a C2H2-type zinc finger transcription factor, was the most abundant (Figure 1D, Figure1—figure supplement 1, Table 1).

To clarify whether the obtained *MLM* genes are involved in the regulation of sphingolipid metabolism, we examined the Myr sensitivity of each gene-knockout homozygous diploid strain. Upon doing so, we found that *com2*Δ, as well as *ypk1*Δ, exhibited Myr sensitivity, while the other *MLM* gene-deficient strains did not (Figure 1E, Figure 1—figure supplement 2).

We further examined the phenotype of *com2*Δ in response to various drugs and stress conditions in addition to Myr. Our results showed that *com2*Δ exhibited higher sensitivity to Myr compared to the wild-type. However, it did not display sensitivity to aureobasidin A (AbA), an inhibitor of inositol phosphoceramide (IPC) synthesis, ergosterol synthesis inhibitors such as miconazole (MCZ) and terbinafine, or any other drugs and stress conditions

162 tested (Figure1—figure supplement 3A-C). Unlike *ypk1*Δ, *com2*Δ does not
163 exhibit sensitivity to AbA. This observation suggests that Com2 plays a more
164 specialized role in regulating sphingolipid biosynthesis at an earlier, upstream
165 step.
166 Next, we analyzed the expression levels of Com2 in wild-type cells under
167 various drug and stress treatment conditions. We observed a remarkable
168 upregulation of Com2 expression under conditions that reduced complex
169 sphingolipid synthesis, such as in Myr-treated cells, AbA-treated cells or Dox-
170 treated *lip1-1* cells (Figure 1F, G). In contrast, inhibition of sterol synthesis did
171 not lead to a significant increase in Com2 expression (Figure 1—figure
172 supplement 3D, E). These findings indicate that Com2 expression is specifically
173 upregulated in response to a reduction in complex sphingolipid levels.
174
175 **Com2 functions upstream of TORC2-Ypk1 pathway**
176 Overexpression of Com2 or Ypk1 suppressed the Myr sensitivity of *lip1-1*
177 (Figure 1D) and deletion of any of these genes conferred Myr sensitivity (Figure
178 1E), suggesting that these two proteins function in the same pathway involved
179 in the regulation of sphingolipid metabolism. Com2 is a C2H2-type zinc finger
180 transcription factor consisting of 443 amino acid residues with two zinc fingers
181 at its C-terminus. In addition to that, several putative phosphorylation sites for
182 AGC kinases, including Ypk1, were found in its amino acid sequence (Figure
183 2A) (Muir et al., 2014). Based on these observations, we hypothesized that
184 Com2 is involved in sphingolipid metabolism downstream of Ypk1 and that
185 Ypk1 impacts the phosphorylation and function of Com2.
186 To test this hypothesis, we investigated the effect of limiting Ypk1 activity on
187 the phosphorylation state of Com2. To this end, we employed *ypk1-as ypk2*Δ
188 cells, which express an ATP analog-sensitive (AS) allele, Ypk1(L424A), and
189 titrated down its activity by addition of an efficacious inhibitor, 1-(tert-butyl)-3-
190 (3-methylbenzyl)-1H-pyrazole[3,4-d]pyrimidin-4-amoine (3-MB-PP1), which
191 has no effect on the wild-type cells (Figure 2B) (Muir et al., 2014). As previously
192 reported (Ishino et al., 2022; Muir et al., 2014), Myr treatment stimulated the
193 phosphorylation of the 3FLAG-tagged Lag1 in wild-type cells, as verified using
194 Phos-tag SDS-PAGE (Figure 2C, lanes 1-5 in the 3FLAG-Lag1 blot), but this

195 effect was abolished in *ypk1-as ypk2*Δ cells (Figure 2C, lanes 7-11 in the
196 3FLAG-Lag1 blot), confirming the inhibition of Ypk1 activity. It is noted that the
197 *ypk1-as ypk2*Δ mutant did not show Myr-dependent phosphorylation of Lag1
198 even in the absence of 3-MB-PP1 (Figure 2C, lane 11 in 3FLAG-Lag1 blot) and
199 was also sensitive to Myr (Figure 2D), suggesting that this mutant appears to
200 be a hypomorphic allele and treatment of 3-MB-PP1 completely blocks Ypk1
201 activity. In contrast to phosphorylation of Lag1, a 13Myc epitope-tagged Com2
202 was highly phosphorylated in both the wild-type and *ypk1-as ypk2*Δ cells
203 (Figure 2C, lanes 1-5 and lanes 7-11 in the Com2-13Myc blot of Phos-tag gel),
204 indicating that the phosphorylation state of Com2 is not dependent on Ypk1
205 activity. Notably, as shown in Figure 1F, G, Myr treatment increased Com2
206 expression in wild-type cells, and this effect was more pronounced in *ypk1-as*
207 *ypk2*Δ cells treated with 3-MB-PP1.
208 Next, we performed an epistatic analysis between *COM2* and *YPK1,*
209 confirming that overexpressing each gene suppressed Myr sensitivity in the
210 corresponding deletion strain. Overexpression of *COM2* did not suppress the
211 Myr sensitivity of *ypk1*Δ cells, whereas overexpression of *YPK1* suppressed the
212 Myr sensitivity of *com2*Δ cells (Figure 2E), indicating that Com2 functions
213 upstream of Ypk1.
214 Taken together, these results suggested that Com2 functions upstream of the
215 TORC2-Ypk1 pathway rather than downstream of it.
216
217 **Com2 expression increases in response to a decrease in sphingolipids**
218 Epistasis analysis suggested that *COM2* functions upstream of *YPK1* (Figure
219 2E). We noticed a putative Com2-binding site (CBS; 5′-CCCTAT-3′) exists in
220 the *YPK1* promoter (Siggers et al., 2014). Based on these observations, we
221 hypothesized that Com2 regulates *YPK1* expression in a sphingolipid-
222 dependent manner (Figure 3A).
223 To test this hypothesis, we performed a time-course analysis of Com2 and
224 Ypk1 during Myr treatment in wild-type and *com2*Δ cells and assessed protein
225 levels by immunoblotting. In wild-type cells, Myr-treatment caused a time-
226 dependent increase in Com2, accompanied by an increase in total Ypk1 as well
227 as enhanced TORC2-dependent phosphorylation of the Ypk1 hydrophobic

228 motif (p-Ypk1^{T662}) (Figure 3B, lanes 1-5, Figure 3C-E). In contrast, in *com2*Δ
229 cells, both the upregulation of Ypk1 and the Myr-dependent increase in p-
230 Ypk1^{T662} were strongly attenuated (Figure 3B, lanes 6–10, Figure 3D, E),
231 indicating that these responses depend on Myr-induced Com2 expression.
232 Notably, TORC2 activity was not reduced in *com2*Δ cells (if anything, it
233 appeared elevated) (Figure 3F), suggesting that the diminished p-Ypk1^{T662}
234 signal primarily reflects decreased Ypk1 abundance rather than defective
235 TORC2 activation.
236 TORC2 senses plasma membrane stress caused by a reduction in complex
237 sphingolipids through the eisosome-associated adaptor proteins, Slm1/2,
238 thereby activating Ypk1 to stimulate sphingolipid synthesis (Figure 1C)
239 (Berchtold et al., 2012). Next, we investigated the contribution of the Slm-
240 TORC2-Ypk1 pathway to the Myr-induced expression of Com2. We observed
241 Myr-induced expression of Com2 even after blocking of the Slm-TORC2-Ypk1
242 pathway at non-permissive temperatures using each temperature-sensitive
243 mutant (Figure 3G), indicating that the induction of Com2 expression upon
244 decreased complex sphingolipids is due to a sensing pathway that is
245 independent from the Slm-TORC2-Ypk1 pathway.
246 Taken together, we demonstrated that Com2 is upregulated in response to a
247 decrease in sphingolipid synthesis, accompanied by upregulation of Ypk1
248 expression and its TORC2-dependent phosphorylation (Figure 3A).
249
250 **Overexpression of Com2 causes increased expression of Ypk1 via a**
251 **putative CBS in the *YPK1* promoter**
252 To further substantiate that Com2 acts upstream of Ypk1, we replaced the
253 endogenous *COM2* promoter with a tetracycline-repressible tet-off promoter by
254 homologous recombination, generating a $P_{\text{tet-off}}$-*GFP-COM2* strain in which
255 Com2 expression can be controlled by Dox (Figure 4A). Using this strain, we
256 assessed Myr sensitivity under conditions of GFP-Com2 overexpression or
257 repression. Cells overexpressing GFP-Com2 (-Dox) were more resistant to Myr
258 than wild-type cells (Figure 4B, upper panel), whereas repression of GFP-Com2
259 (+Dox) rendered cells as Myr-sensitive as *com2*Δ cells (Figure 4B, lower panel).

260 A putative Com2-binding site (CBS) was identified in the *YPK1* promoter
261 (Figure 4C). In addition, a genome-wide search of the *S. cerevisiae* genome
262 using the CBS consensus motif revealed a matching sequence in the promoter
263 of *LCB1*, which encodes a catalytic subunit of SPT (Figure 4C; Figure 4—figure
264 supplement 1). To test whether Com2 directly regulates *YPK1* and *LCB1*
265 expression, we examined the effects of GFP-Com2 overexpression on their
266 expression levels. Induction of GFP-Com2 overexpression (-Dox) markedly
267 increased Ypk1 abundance, and also led to a significant, albeit more modest,
268 increase in Lcb1 abundance (Figure 4D, E, Figure 4—figure supplement 2).
269 We next constructed *lacZ* reporters driven by the *YPK1* or *LCB1* promoter
270 (Figure 4C) and assessed promoter activity by measuring β-galactosidase
271 activity. Compared with conditions in which GFP-Com2 was repressed (+Dox),
272 GFP-Com2 induction (-Dox) increased β-galactosidase activity ~6-fold for the
273 *YPK1* promoter and ~2.5-fold for the *LCB1* promoter (Figure 4F). Notably, this
274 Com2-dependent activation was abolished by deleting the CBS from each
275 promoter, indicating that Com2 directly stimulates *YPK1* and *LCB1* transcription
276 via the CBS motif. Collectively, these findings support a model in which Com2
277 contributes to sphingolipid metabolism by transcriptionally upregulating *YPK1*
278 and *LCB1*.
279
280 **Com2 promotes sphingolipid synthesis, partly through the expression of**
281 **Ypk1**
282 To test whether Com2 directly regulates *YPK1* transcription and how this
283 regulation impacts sphingolipid metabolism, we used CRISPR-Cas9 genome
284 editing to delete the putative Com2-binding site (CBS) from the endogenous
285 *YPK1* promoter, generating P_{YPK1}-Δ*CBS* cells (Fig. 5A).
286 We first assessed the Myr sensitivity of P_{YPK1}-Δ*CBS* cells. P_{YPK1}-Δ*CBS* cells
287 were more sensitive to Myr than wild-type cells, but less sensitive than *com2*Δ
288 cells or doxycycline-treated $P_{\text{tet-off}}$-*GFP-COM2* cells (+Dox) (Figure 5B, C).
289 We next examined Ypk1 expression in P_{YPK1}-Δ*CBS* cells by western blotting.
290 Under Myr-treated conditions, Com2-13Myc levels were comparable between
291 wild-type and P_{YPK1}-Δ*CBS* cells, whereas Ypk1 levels were reduced in P_{YPK1}-
292 Δ*CBS* cells relative to wild-type and were similar to those in *com2*Δ cells (Figure

293 5D–F). Consistently, TORC2-dependent phosphorylation at the hydrophobic
294 motif (p-Ypk1^{T662}) was decreased in P_{YPK1}-Δ*CBS* cells compared with wild-type
295 and was comparable to that in *com2*Δ cells (Figure 5D, G).
296 We then performed TLC analysis to examine how Com2-dependent regulation
297 influences sphingolipid synthesis. Consistent with the Myr resistant phenotype,
298 overexpression of GFP-Com2 (-Dox) significantly increased sphingolipid levels
299 under both untreated (Figure 5H, lane 1 vs. lane 5) and Myr-treated conditions
300 (Figure 5H, lane 6 vs. lane 10). In contrast, under Myr treatment, sphingolipid
301 levels were substantially reduced in *com2*Δ cells and in GFP-Com2-repressed
302 (+Dox) cells compared with wild-type (Figure 5H, lane 6 vs. lane 7 or 9). In Myr-
303 treated P_{YPK1}-Δ*CBS* cells, sphingolipid levels were significantly lower than in
304 GFP-Com2-overexpressing (-Dox) cells (Figure 5H, lane 8 vs. lane 10), but only
305 slightly reduced compared with wild-type (Figure 5H, lane 6 vs. lane 8),
306 consistent with the intermediate Myr sensitivity of P_{YPK1}-Δ*CBS* cells (Figure 5B).
307 Notably, the double mutant P_{YPK1}-*ΔCBS* and P_{LCB1}-*ΔCBS* (in which the CBS
308 sequence was deleted from the *LCB1* promoter) did not exhibit Myr sensitivity
309 comparable to that of *com2*Δ (Figure 5—figure supplement A-C).
310 Taken together, these results suggest that Ypk1 represent a major Com2
311 target under sphingolipid-depleted conditions, although additional Com2-
312 dependent targets likely contribute to sphingolipid homeostasis.
313
314 **Mapping *COM2* regulatory regions required for sphingolipid-dependent**
315 **Com2 expression**
316 To identify the regions required for Com2 expression control, we constructed
317 a series of plasmids carrying stepwise deletions in either the ~500 bp 5′
318 upstream region (putative *COM2* promoter) or the *COM2* ORF (Figure 6A).
319 These plasmids were introduced into *com2*Δ cells, and we compared Myr
320 sensitivity and Com2 protein abundance in the presence or absence of Myr
321 (Figure 6). Whereas *com2*Δ cells were Myr-sensitive, introduction of most
322 plasmids restored Myr resistance to varying degrees (Figure 6B). In contrast,
323 the Δ2-190 mutant and truncation mutants lacking the DNA region
324 corresponding to the Zn-finger domain (1-379, 1-230, 1-143, 1-87) failed to
325 complement Myr sensitivity.

326 We next examined the expression of these mutants by immunoblotting. For
327 the promoter-deletion series, removal of ≥180 bp from the 5′ upstream region
328 caused a marked reduction in basal Com2 abundance. Nevertheless, all
329 promoter-deletion constructs still showed a clear increase in Com2 levels upon
330 Myr treatment (Figure 6C). Consistently, in a strain in which the endogenous
331 *COM2* promoter was replaced with a tet-off promoter ($P_{tet\text{-}off}$-*13Myc-COM2*),
332 Com2 levels increased over time after Myr addition both under "induced (-Dox)"
333 and "repressed (+Dox)" conditions (Figure 6—supplement 1). These results
334 suggest that Myr-dependent upregulation of Com2 is not primarily driven by the
335 native promoter.
336 In contrast, stepwise deletions within the *COM2* ORF revealed a prominent
337 effect on Com2 abundance. Deletion of ≥40 amino acids from the N-terminus
338 caused a strong accumulation of Com2 protein irrespective of Myr treatment
339 (Figure 6D). A C-terminal truncation removing 213 residues (1-230) still
340 exhibited Myr-dependent induction, whereas more extensive C-terminal
341 truncations (1-143 and 1-87) accumulated to high levels regardless of Myr
342 (Figure 6E). Together, these findings indicate that Com2 expression control is
343 largely determined by sequences within the ORF, rather than by the promoter.
344

345 **Com2 is rapidly degraded by the ubiquitin-proteasome system in**
346 **response to increased sphingolipid levels**

347 Because Com2 abundance increases upon Myr-induced sphingolipid
348 depletion and this response is independent of the promoter, we next asked
349 whether increasing intracellular sphingolipids would conversely downregulate
350 Com2. Three hours after Myr treatment, we added phytosphingosine (PHS), a
351 ceramide precursor, to bypass the blocked step and restore sphingolipid
352 synthesis (Figure 7A). Com2 levels, which were elevated by Myr, dropped
353 rapidly within 1 hr of PHS addition (Figure 7B, C). In contrast, Ypk1 levels also
354 increased upon Myr treatment but did not show a significant decrease after PHS
355 addition (Figure 7B, D). Notably, TORC2-dependent phosphorylation of Ypk1
356 (p-Ypk1^{T662}) increased over time during Myr treatment and declined promptly
357 after PHS addition (Figure 7B, E). These results suggest that Com2 abundance
358 is dynamically tuned to intracellular sphingolipid levels.

359 To pinpoint the biosynthetic step responsible for the PHS-dependent reduction
360 in Com2, we used loss-of-function mutants and step-specific inhibitors targeting
361 distinct stages of sphingolipid synthesis (Figure 7A). Blocking
362 mannnosyldiinositol phosphorylceramide, $M(IP)_2C$ synthesis (*ipt1*Δ) did not
363 impair the PHS-dependent decrease in Com2, which remained comparable to
364 that in wild-type cells (Figure 7F, G). By contrast, inhibiting ceramide synthesis
365 (*lip1-1* +Dox), IPC synthesis (*aur1-19* +AbA), or mannnosylinositol
366 phosphrylceramide, MIPC synthesis (*csg2*Δ) abolished the PHS-dependent
367 reduction in Com2 (Figure 7F, G). Thus, Com2 downregulation requires flux
368 through the pathway up to MIPC. The rapid PHS-induced change in Com2
369 expression correlated with changes in p-Ypk1^{T662} levels in wild-type cells and
370 in mutants impaired at different steps of sphingolipid metabolism, except for
371 those in *csg2*Δ cells (Figure 7F, H).
372 We next considered that the rapid loss of Com2 following PHS addition might
373 reflect regulated protein degradation, such as proteasomal degradation or
374 autophagy. Co-treatment with the proteasome inhibitors MG132 and
375 bortezomib markedly suppressed the PHS-dependent decrease in Com2 and
376 led to the appearance of high-molecular-weight species consistent with
377 polyubiquitinated Com2 (Figure 7I, J). In contrast, deletion of *ATG5*, which is
378 essential for autophagosome formation, did not prevent the PHS-dependent
379 decrease in Com2 (Figure 7—figure supplement). Together, these data indicate
380 that Com2 is downregulated primarily through ubiquitin-proteasome system
381 (UPS)-dependent degradation.
382 In summary, our results support a model in which an increase in the complex
383 sphingolipids triggers UPS-dependent degradation of Com2, thereby providing
384 negative feedback to restrain downstream sphingolipid synthesis (Figure 7K).
385
386 **Identification of Com2 ubiquitination sites and the role of phosphorylation**
387 **in sphingolipid-dependent Com2 degradation**
388 Because deletion of amino acids 2-40 markedly increased Com2 expression
389 levels (Figure 6D), we hypothesized that this region is involved in PHS-
390 dependent degradation. Consistent with this idea, PHS-dependent degradation

391 of Com2 was completely abolished in the mutant lacking amino acids 2-40
392 (Figure 8A).
393 To identify ubiquitination sites, lysine residues located within or near this
394 region were substituted with arginine (Figure 8B). Mutation of K23 and K35,
395 either individually or together, or mutation of K51 alone, did not affect PHS-
396 dependent degradation. In contrast, simultaneous mutation of K23, K35, and
397 K51 (KR mutant) significantly suppressed PHS-induced degradation (Figure
398 8C-E). The KR mutant fully complemented the Myr sensitivity of the *com2*Δ
399 strain, indicating that these substitutions do not impair Com2 function (Figure
400 8—figure supplement 1A). Notably, the KR mutant exhibited a PHS-induced
401 mobility shift that was reversed by λphosphatase (λPPase) treatment, indicating
402 phosphorylation-dependent modification (Figure 8F). These results suggest
403 that ubiquitination at K23, K35, and K51 promotes proteasome-dependent
404 degradation of Com2.
405 Because degradation was suppressed in the KR mutant despite increased
406 phosphorylation, we next examined the role of phosphorylation in Com2
407 stability. Phos-tag SDS-PAGE resolved several phosphorylated Com2 species
408 that shifted downward following λPPase treatment, demonstrating that Com2 is
409 highly phosphorylated (Figure 8G, lanes 1, 2).
410 In addition to the five phosphorylation sites annotated in the Saccharomyces
411 Genome Database, we identified five predicted AGC kinase target sites,
412 including putative Ypk1 phosphorylation sites, yielding a total of ten candidate
413 phosphorylation sites (Fig. 8—figure supplement 1B). Progressive substitution
414 of these serine/threonine residues with alanine (ST-A3 to ST-A10) caused
415 stepwise reduction of phosphorylation-dependent band shifts, with ST-A10
416 showing a marked loss of phosphorylation (Figure 8G, lanes 2-7).
417 Consistent with this result, PHS-dependent degradation was unchanged in
418 ST-A3 but progressively suppressed in mutants containing five or more
419 substitutions and was significantly reduced in ST-A10 (Figure 8H-J). Together,
420 these results indicate that phosphorylation of Com2 is required for its PHS-
421 dependent degradation.
422
423

Discussion

Bilayer assembly during membrane biogenesis requires the coordinated supply and organization of multiple lipid species, necessitating integrated control of lipid synthesis, uptake, metabolism, and subcellular distribution (Nohturfft and Zhang, 2009). Global regulation of lipid metabolism is achieved not only through signaling pathways that modulate the activity of lipid metabolic enzymes, but also through master transcriptional regulators that coordinate expression of genes encoding these enzymes and their modulators. Master transcriptional regulators have been identified for glycerophospholipids, lipid-saturation control, and sterol metabolism in both yeast and mammals (Covino et al., 2018; Nohturfft and Zhang, 2009). In contrast, although sphingolipid metabolic flux is well understood to be regulated through the TORC2-Ypk1 pathway via control of biosynthetic enzyme activity (Berchtold et al., 2012), transcriptional mechanisms governing sphingolipid metabolism remain far less defined (Breslow and Weissman, 2010).

In this study, we show that Com2 functions as a master transcriptional regulator of sphingolipid metabolism in budding yeast by responding to reduced sphingolipid levels, upregulating its own expression, and promoting Ypk1 expression to stimulate sphingolipid synthesis.

Previous work reported that *com2*Δ cells are hypersensitive to sulfur dioxide (SO_2) and that Com2 acts as a major transcription factor controlling expression of genes required for SO_2 tolerance (Lage et al., 2019). Com2 has also been identified as a regulator of the UASru element within the promoter of *IME1*, the master regulator of meiosis in budding yeast, where deletion of this element markedly reduces *IME1* transcription (Kahana-Edwin et al., 2013). How the Com2-dependent program uncovered here intersects with these pathways remains unclear; however, Com2 may employ shared regulatory logic across distinct physiological responses, an idea that will be important to address in future studies.

YPK1 is a major Com2 target, but additional targets likely contribute to sphingolipid homeostasis

456 Our data show that *YPK1* is one of the major transcriptional targets of Com2
457 in sphingolipid metabolism. A genome-wide search based on the Com2-binding
458 site (CBS) consensus sequence also identified a CBS-like element in the
459 promoter of *LCB1*, which encodes a catalytic subunit of SPT, and a *LacZ*
460 reporter assay further suggested that the *LCB1* promoter can respond to Com2.
461 Notably, deletion of the CBS from the *YPK1* promoter (P_{YPK1}-ΔCBS) reduced
462 Myr-induced Ypk1 upregulation to a level comparable to that seen in *com2*Δ
463 cells (Figure 5D). However, this promoter mutant did not phenocopy the strong
464 Myr sensitivity of *com2*Δ. Likewise, a double mutant lacking CBS elements in
465 both the *YPK1* and *LCB1* promoters failed to recapitulate the *com2*Δ phenotype
466 (Figure 5—figure supplement). Together, these results suggest that, in addition
467 to *YPK1* and *LCB1*, Com2 likely controls other target genes that collectively
468 contribute to sphingolipid homeostasis.
469

470 **Com2 degradation is triggered by a cellular readout of complex**
471 **sphingolipids**

472 Com2 levels increased when sphingolipid synthesis was reduced by Myr
473 treatment, whereas exogenous addition of phytosphingosine (PHS), a
474 ceramide precursor, rapidly promoted Com2 degradation via the ubiquitin-
475 proteasome system (UPS) (Figure 7B, I). Systematic inhibition of individual
476 steps in the sphingolipid pathway further suggested that the PHS-dependent
477 degradation signal reflects the status of complex sphingolipids at or
478 downstream of MIPC (Figure 7F). In glycerophospholipid and sterol metabolism,
479 several lipid-sensing transcriptional systems are well established—for example,
480 Opi1 sensing phosphatidic acid (Loewen et al., 2004), Mga2/Spt23 sensing
481 membrane lipid saturation to control *OLE1* expression (Ballweg et al., 2020;
482 Romanauska and Köhler, 2021), and Upc2 sensing sterol depletion to induce
483 sterol biosynthetic genes (Yang et al., 2015). In contrast, the molecular
484 mechanisms by which cells sense sphingolipid levels, particularly complex
485 sphingolipids, remain poorly understood (Breslow and Weissman, 2010).
486 TORC2-Ypk1 signaling is also thought to be influenced by complex sphingolipid
487 status (Figure 7F, H), yet the identity of the upstream sensor is still unclear.
488 Thus, dissecting the mechanism of Com2 degradation may provide a tractable

489 entry point to uncover the elusive sphingolipid sensor operating at the top of
490 this pathway.
491
492 **How are Com2 ubiquitination and degradation controlled?**
493 Many transcription factors are regulated through proteolysis by the UPS in
494 response to environmental and metabolic cues, including oxidative stress, heat
495 shock, nutrient limitation, changes in cellular redox status, and shifts in
496 metabolic state (e.g., glucose availability, AMP/ATP, NAD^+/NADH, and TCA-
497 cycle metabolites) (Geng et al., 2012). Within the UPS, E3 ubiquitin ligases act
498 as central decision-makers that determine whether a substrate is degraded. In
499 many cases, this decision is implemented through the recognition of degron
500 motifs and their modulation by post-translational modifications, thereby
501 converting stress/metabolic signals into changes in protein half-life (Finley et
502 al., 2012).
503 Here, we found that PHS-induced degradation of Com2 critically depends on
504 its N-terminal region (notably the segment around residues 2-40) (Figure 8A).
505 Moreover, substitution of lysine residues near the N terminus with arginine
506 (K23R, K35R, and K51R; hereafter the KR mutant) markedly attenuated PHS-
507 dependent Com2 degradation. These observations suggest that the N-terminal
508 region may provide ubiquitin-acceptor lysines and/or serve as a degron that is
509 recognized by an E3 ubiquitin ligase.
510 Notably, the KR mutant displayed an increased phosphorylation signal after
511 PHS treatment (Figure 8F). In budding yeast, the transcription factor Gcn4 is
512 phosphorylated by Pho85 under non-starvation conditions, which generates a
513 phosphodegron that is recognized by SCF^{Cdc4}, leading to ubiquitination and
514 proteasomal degradation (Meimoun et al., 2000). By analogy, Com2
515 phosphorylation may similarly act as a trigger for UPS-dependent degradation,
516 potentially by creating or exposing a phosphodegron. Consistent with this idea,
517 a mutant in which multiple predicted phosphorylation sites were collectively
518 replaced (ST-A10) exhibited reduced phosphorylation and a significant
519 suppression of PHS-dependent degradation (Figure 8G-J). Together, these
520 results support a model in which Com2 phosphorylation is an important
521 upstream step in its degradation. Nevertheless, the increased phosphorylation

522 observed in the KR mutant could also reflect accumulation of phosphorylated
523 Com2 due to impaired turnover, and future work will be required to establish
524 the causal order of phosphorylation and ubiquitination.
525 Based on these findings, we propose the model shown in Figure 9. When
526 intracellular sphingolipid levels are low, Com2 is stabilized and promotes
527 sphingolipid synthesis by upregulating genes that positively regulate the
528 pathway and contain Com2-binding sites (CBS), such as *YPK1* and *LCB1*.
529 Conversely, when sphingolipid levels are high, an as-yet-unidentified complex
530 sphingolipid sensor and downstream signaling pathway may promote Com2
531 phosphorylation, recruit an E3 ubiquitin ligase, and drive Com2 ubiquitination
532 followed by rapid proteasomal degradation.
533
534 **Is transcriptional control of sphingolipid metabolism evolutionarily**
535 **conserved?**
536 Whether a Com2-like mechanism of sphingolipid metabolic control is
537 evolutionarily conserved in mammals remains an open question. In mice,
538 ZFP750 (ZNF750 in humans) has been reported to function as a master
539 regulator of ceramide synthase genes, particularly in the skin, where it is
540 essential for establishing epidermal barrier function by maintaining proper lipid
541 composition (Butera et al., 2023). ZFP750 directly binds to the promoters of
542 lipid metabolic enzyme genes, including Elovl6 and Elovl7, which are involved
543 in fatty acid elongation, thereby regulating lipid metabolism at the transcriptional
544 level.
545 Although Com2 cannot be considered a clear ortholog of ZFP750, it is
546 tempting to speculate that ZFP750 may also be subject to functional regulation
547 linked to sphingolipid levels, analogous to that observed for Com2. Notably,
548 more than 700 C2H2-type zinc finger proteins are annotated in the human
549 genome (Nabeel-Shah et al., 2024), raising the possibility that additional
550 transcription factors may regulate sphingolipid metabolism in a manner similar
551 to Com2.
552 Our findings therefore provide a conceptual framework for understanding
553 sphingolipid homeostasis as a transcriptionally controlled process that may be
554 conserved beyond yeast.
555

556 **Materials and Methods**

557 **Strains, plasmids, and media**

558 Descriptions of the strains and plasmids used in this study are presented in
559 Tables 2 and Table 3. *Escherichia coli* DH5α or JM109 was used as the
560 bacterial host for plasmid construction. Coding sequences were amplified by
561 means of PCR, using KOD-Plus-Neo polymerase (Toyobo) or PrimeSTAR®
562 GXL polymerase (TaKaRa Bio Inc.). The plasmids were sequenced to ensure
563 that no mutations were introduced owing to the manipulation. Mutant constructs
564 were generated using site-directed mutagenesis and confirmed using
565 sequencing. The media used for yeast culture were YPD (1% yeast extract, 2%
566 peptone, and 2% glucose) or synthetic dextrose (SD) medium (2% glucose and
567 0.67% yeast nitrogen base without amino acids). Appropriate amino acids and
568 bases were added to the SD medium, as necessary. Yeast cells were cultured
569 at 26°C, unless otherwise stated. All deletion and tagged strains were
570 constructed using homologous recombination with PCR-generated DNA
571 fragments, as described previously (Longtine et al., 1998). Multiple-mutant
572 strains of *S. cerevisiae* were generated by genetic crossing of the respective
573 single-mutant strains followed by tetrad dissection analysis.

574

575 **Yeast growth assays**

576 For the yeast plate growth assay, cells were adjusted to an OD_{600} of 1.0,
577 serially diluted in fourfold steps, and 5 μL of each dilution was spotted onto
578 assay plates. Plates were incubated at the indicated temperature for 3-4 days
579 and then photographed.

580 For the liquid growth assay, as described previously (Ishino et al., 2022), cells
581 were inoculated into YPD medium or YPD supplemented with Myr at an initial
582 OD_{600} of 0.1. Growth was monitored every 30 min at 26°C using a microplate
583 reader (Tecan Sunrise, Tecan Japan, Co., Ltd, Kanagawa, Japan) with three
584 biological replicates.

585

586 **Antibody production**

587 The rabbit polyclonal antibody that recognizes Com2 was produced as follows.
588 A His_6-fused Com2 protein was expressed in *E. coli* Rosetta-gami B (DE3)

589 pLysS cells and the total cell lysate was separated on an SDS-PAGE gel. The
590 band corresponding to the His_6-Com2 fusion protein was excised from the SDS-
591 PAGE gel and electroeluted from the gel slices using an AE-3590
592 electrochamber (Atto). An aliquot of approximately 300 μg of the fusion protein
593 was emulsified with Freund's complete adjuvant and injected intramuscularly
594 or subcutaneously into young female Japanese white rabbits. Antisera were
595 purified using an affinity column immobilized with His_6-ProS2-Com2 (382-443
596 a.a.) fusion protein.
597
598 **Western blot**
599 Protein extracts were prepared using the TCA precipitation method, loaded
600 onto normal or Phos-tag SDS-PAGE gels, and transferred to PVDF
601 membranes (Fujifilm Wako). λPPase treatment was performed as described
602 previously (Ishino et al., 2022). The antibodies and dilutions used in this study
603 were listed in Table 4.
604
605 **Sphingolipid analysis**
606 Sphingolipids were extracted from *S. cerevisiae* and analyzed using TLC, as
607 described previously (Yamaguchi et al., 2018).
608
609 **Construction of *LacZ* reporter plasmids**
610 The fragments containing the promoter regions of *YPK1* and *LCB1* were
611 amplified by means of PCR and cloned into the XhoI and BamHI sites of the
612 4×*CDRE-LacZ* fusion plasmid, pAMS366 (Stathopoulos and Cyert, 1997)
613 (gifted by Dr. Martha Cyert, Stanford University) using the In-Fusion® Cloning
614 Kit (Clontech), resulting in pP_{YPK1}-*LacZ* and pP_{LCB1}-*LacZ* reporter plasmids,
615 respectively.
616
617 **Genome editing for generation of the P_{YPK1}-Δ*CBS* strain**
618 The pMT1447 plasmid, constructed from the pSpCas9(BB)-2A-GFP plasmid
619 (Ran et al., 2013) combined with the Z_4EV expression system (McIsaac et al.,
620 2013), co-expresses the nuclease protein Cas9 and gRNA, which guides the
621 Cas9 protein with the target promoter sequence of *YPK1*. The repair DNA

622 fragment was amplified from pNK19 carrying the P_{YPK1}-Δ*CBS* fragment. The
623 yeast wild-type strain was co-transformed with the pMT1603 plasmid and the
624 repair DNA fragment using the lithium acetate transformation method. After
625 selecting the uracil prototrophic transformants, the genomic DNA purified from
626 the yeast transformants was used for genotyping by means of PCR using
627 specific primers, to confirm the deletion of the CBS in the chromosomal *YPK1*
628 promoter. The pMT1603 plasmid was lost by means of 5-FOA counter
629 selection.
630
631 **Statistical analysis**
632 Statistical analysis was performed using Prism 10 (GraphPad) or Excel
633 (Microsoft) software, and the specific tests carried out have been mentioned in
634 the text and figure legends.
635
636 **Acknowledgments**
637 We express our deep appreciation to Prof. Scott D. Emr for generously
638 providing the plasmids and strains. We thank Profs. Isamu Kameshita and
639 Noriyuki Sueyoshi for providing the λPPase-expressing plasmid. We also thank
640 Prof. Martha Cyert for providing the *LacZ* reporter plasmid, pAMS366. We also
641 appreciate Prof. Takayuki Sekito for his technical advice on the experimental
642 methods. We acknowledge the technical expertise of the DNA Core Facility of
643 the Gene Research Center, Kagawa University. This work was supported by
644 JSPS KAKENHI grant numbers JP19K05828, 23K26835 (to M.Tabuchi).
645
646 **Author contributions**
647 Mitsuaki Tabuchi designed the research; Kosei Matsumoto, Ayane Nagai, Nao
648 Komatsu, Yuko Ishino, Rina Shirai, Toshiya Ueno, Mio Masaki, and Mitsuaki
649 Tabuchi performed the research; Kosei Matsumoto, Ayane Nagai, Nao
650 Komatsu, Yuko Ishino, Rina Shirai, and Mitsuaki Tabuchi analyzed the data;
651 Kosei Matsumoto, Ayane Nagai, and Mitsuaki Tabuchi wrote the manuscript;
652 Motohiro Tani, Tatsuya Maeda, Naotaka Tanaka, and Ken-taro Sakata
653 reviewed and edited the manuscript; Tatsuya Maeda provided resources; and

Mitsuaki Tabuchi supervised the study and was responsible for funding acquisition and project administration.

657 **References**

658 Ambroziak J, Henry SA. 1994. *INO2* and *INO*4 gene products, positive
659 regulators of phospholipid biosynthesis in *Saccharomyces cerevisiae*,
660 form a complex that binds to the *INO1* promoter. Journal of Biological
661 Chemistry **269**:15344–15349. DOI: https://doi.org/10.1016/S0021-
662 9258(17)36612-7
663 Audhya A, Loewith R, Parsons AB, Gao L, Tabuchi M, Zhou H, Boone C, Hall
664 MN, Emr SD. 2004. Genome-wide lethality screen identifies new
665 PI4,5P2 effectors that regulate the actin cytoskeleton. The EMBO
666 Journal **23**:3747–3757. DOI: https://doi.org/10.1038/sj.emboj.7600384
667 Ballweg S, Sezgin E, Doktorova M, Covino R, Reinhard J, Wunnicke D,
668 Hänelt I, Levental I, Hummer G, Ernst R. 2020. Regulation of lipid
669 saturation without sensing membrane fluidity. Nature Communications
670 **11**:756. DOI: https://doi.org/10.1038/s41467-020-14528-1
671 Berchtold D, Piccolis M, Chiaruttini N, Riezman I, Riezman H, Roux A,
672 Walther TC, Loewith R. 2012. Plasma membrane stress induces
673 relocalization of Slm proteins and activation of TORC2 to promote
674 sphingolipid synthesis. Nature Cell Biology **14**:542–547. DOI:
675 https://doi.org/10.1038/ncb2480
676 Breslow DK, Collins SR, Bodenmiller B, Aebersold R, Simons K, Shevchenko
677 A, Ejsing CS, Weissman JS. 2010. Orm family proteins mediate
678 sphingolipid homeostasis. Nature **463**:1048–1053. DOI:
679 https://doi.org/10.1038/nature08787
680 Breslow DK, Weissman JS. 2010. Membranes in Balance: Mechanisms of
681 Sphingolipid Homeostasis. Molecular Cell **40**:267–279. DOI:
682 https://doi.org/10.1016/j.molcel.2010.10.005
683 Butera A, Agostini M, Cassandri M, De Nicola F, Fanciulli M, D'Ambrosio L,
684 Falasca L, Nardacci R, Wang L, Piacentini M, Knight RA, Jia W, Sun
685 Q, Shi Y, Wang Y, Candi E, Melino G. 2023. ZFP750 affects the
686 cutaneous barrier through regulating lipid metabolism. Science
687 Advances **9**:eadg5423. DOI: https://doi.org/10.1126/sciadv.adg5423
688 Covino R, Hummer G, Ernst R. 2018. Integrated Functions of Membrane
689 Property Sensors and a Hidden Side of the Unfolded Protein
690 Response. Molecular Cell **71**:458–467. DOI:
691 https://doi.org/10.1016/j.molcel.2018.07.019
692 Eltschinger S, Loewith R. 2016. TOR Complexes and the Maintenance of
693 Cellular Homeostasis. Trends in Cell Biology **26**:148–159. DOI:
694 https://doi.org/10.1016/j.tcb.2015.10.003
695 Finley D, Ulrich HD, Sommer T, Kaiser P. 2012. The Ubiquitin–Proteasome
696 System of *Saccharomyces cerevisiae*. Genetics **192**:319–360. DOI:
697 https://doi.org/10.1534/genetics.112.140467
698 Geng F, Wenzel S, Tansey WP. 2012. Ubiquitin and Proteasomes in
699 Transcription. Annual Review of Biochemistry **81**:177–201. DOI:
700 https://doi.org/10.1146/annurev-biochem-052110-120012
701 Goldstein JL, DeBose-Boyd RA, Brown MS. 2006. Protein Sensors for
702 Membrane Sterols. Cell **124**:35–46. DOI:
703 https://doi.org/10.1016/j.cell.2005.12.022
704 Gururaj C, Federman R, Chang A. 2013. Orm Proteins Integrate Multiple
705 Signals to Maintain Sphingolipid Homeostasis. Journal of Biological

Chemistry **288**:20453–20463. DOI: https://doi.org/10.1074/jbc.M113.472860

Harayama T, Riezman H. 2018. Understanding the diversity of membrane lipid composition. Nature Reviews Molecular Cell Biology **19**:281–296. DOI: https://doi.org/10.1038/nrm.2017.138

Hua X, Sakai J, Brown MS, Goldstein JL. 1996. Regulated Cleavage of Sterol Regulatory Element Binding Proteins Requires Sequences on Both Sides of the Endoplasmic Reticulum Membrane. Journal of Biological Chemistry **271**:10379–10384. DOI: https://doi.org/10.1074/jbc.271.17.10379

Ishino Y, Komatsu N, Sakata K, Yoshikawa D, Tani M, Maeda T, Morishige K, Yoshizawa K, Tanaka N, Tabuchi M. 2022. Regulation of sphingolipid biosynthesis in the endoplasmic reticulum via signals from the plasma membrane in budding yeast. The FEBS Journal **289**:457–472. DOI: https://doi.org/10.1111/febs.16189

Kahana-Edwin S, Stark M, Kassir Y. 2013. Multiple MAPK Cascades Regulate the Transcription of *IME1*, the Master Transcriptional Activator of Meiosis in Saccharomyces cerevisiae. PLoS ONE **8**:e78920. DOI: https://doi.org/10.1371/journal.pone.0078920

Kwiatek JM, Han G-S, Carman GM. 2020. Phosphatidate-mediated regulation of lipid synthesis at the nuclear/endoplasmic reticulum membrane. Biochimica et Biophysica Acta (BBA) - Molecular and Cell Biology of Lipids **1865**:158434. DOI: https://doi.org/10.1016/j.bbalip.2019.03.006

Lage P, Sampaio-Marques B, Ludovico P, Mira NP, Mendes-Ferreira A. 2019. Transcriptomic and chemogenomic analyses unveil the essential role of Com2-regulon in response and tolerance of *Saccharomyces cerevisiae* to stress induced by sulfur dioxide. Microbial Cell **6**:509–523. DOI: https://doi.org/10.15698/mic2019.11.697

Loewen CJR. 2003. A conserved ER targeting motif in three families of lipid binding proteins and in Opi1p binds VAP. The EMBO Journal **22**:2025–2035. DOI: https://doi.org/10.1093/emboj/cdg201

Loewen CJR, Gaspar ML, Jesch SA, Delon C, Ktistakis NT, Henry SA, Levine TP. 2004. Phospholipid Metabolism Regulated by a Transcription Factor Sensing Phosphatidic Acid. Science **304**:1644–1647. DOI: https://doi.org/10.1126/science.1096083

Longtine MS, Mckenzie Iii A, Demarini DJ, Shah NG, Wach A, Brachat A, Philippsen P, Pringle JR. 1998. Additional modules for versatile and economical PCR-based gene deletion and modification in *Saccharomyces cerevisiae*. Yeast **14**:953–961. DOI: https://doi.org/10.1002/(SICI)1097-0061(199807)14:10%3C953::AID-YEA293%3E3.0.CO;2-U

McIsaac RS, Oakes BL, Wang X, Dummit KA, Botstein D, Noyes MB. 2013. Synthetic gene expression perturbation systems with rapid, tunable, single-gene specificity in yeast. Nucleic Acids Research **41**:e57–e57. DOI: https://doi.org/10.1093/nar/gks1313

Meimoun A, Holtzman T, Weissman Z, McBride HJ, Stillman DJ, Fink GR, Kornitzer D. 2000. Degradation of the Transcription Factor Gcn4 Requires the Kinase Pho85 and the SCFCDC4 Ubiquitin–Ligase

754 Complex. Molecular Biology of the Cell **11**:915–927. DOI:
755 https://doi.org/10.1091/mbc.11.3.915, PMID: 10712509
756 Muir A, Ramachandran S, Roelants FM, Timmons G, Thorner J. 2014.
757 TORC2-dependent protein kinase Ypk1 phosphorylates ceramide
758 synthase to stimulate synthesis of complex sphingolipids. eLife
759 **3**:e03779. DOI: https://doi.org/10.7554/eLife.03779
760 Nabeel-Shah S, Pu S, Burns JD, Braunschweig U, Ahmed N, Burke GL, Lee
761 H, Radovani E, Zhong G, Tang H, Marcon E, Zhang Z, Hughes TR,
762 Blencowe BJ, Greenblatt JF. 2024. C2H2-zinc-finger transcription
763 factors bind RNA and function in diverse post-transcriptional regulatory
764 processes. Molecular Cell **84**:3810-3825.e10. DOI:
765 https://doi.org/10.1016/j.molcel.2024.08.037
766 Niles BJ, Mogri H, Hill A, Vlahakis A, Powers T. 2012. Plasma membrane
767 recruitment and activation of the AGC kinase Ypk1 is mediated by
768 target of rapamycin complex 2 (TORC2) and its effector proteins Slm1
769 and Slm2. Proceedings of the National Academy of Sciences
770 **109**:1536–1541. DOI: https://doi.org/10.1073/pnas.1117563109
771 Nohturfft A, Brown MS, Goldstein JL. 1998. Sterols regulate processing of
772 carbohydrate chains of wild-type SREBP cleavage-activating protein
773 (SCAP), but not sterol-resistant mutants Y298C or D443N.
774 Proceedings of the National Academy of Sciences **95**:12848–12853.
775 DOI: https://doi.org/10.1073/pnas.95.22.12848
776 Nohturfft A, DeBose-Boyd RA, Scheek S, Goldstein JL, Brown MS. 1999.
777 Sterols regulate cycling of SREBP cleavage-activating protein (SCAP)
778 between endoplasmic reticulum and Golgi. Proceedings of the National
779 Academy of Sciences **96**:11235–11240. DOI:
780 https://doi.org/10.1073/pnas.96.20.11235
781 Nohturfft A, Yabe D, Goldstein JL, Brown MS, Espenshade PJ. 2000.
782 Regulated Step in Cholesterol Feedback Localized to Budding of
783 SCAP from ER Membranes. Cell **102**:315–323. DOI:
784 https://doi.org/10.1016/S0092-8674(00)00037-4
785 Nohturfft A, Zhang SC. 2009. Coordination of Lipid Metabolism in Membrane
786 Biogenesis. Annual Review of Cell and Developmental Biology **25**:539–
787 566. DOI: https://doi.org/10.1146/annurev.cellbio.24.110707.175344
788 Ran FA, Hsu PD, Wright J, Agarwala V, Scott DA, Zhang F. 2013. Genome
789 engineering using the CRISPR-Cas9 system. Nature Protocols
790 **8**:2281–2308. DOI: https://doi.org/10.1038/nprot.2013.143
791 Rawson RB, Zelenski NG, Nijhawan D, Ye J, Sakai J, Hasan MT, Chang TY,
792 Brown MS, Goldstein JL. 1997. Complementation Cloning of , a Gene
793 Encoding a Putative Metalloprotease Required for Intramembrane
794 Cleavage of SREBPs. Molecular Cell **1**:47–57. DOI:
795 https://doi.org/10.1016/S1097-2765(00)80006-4
796 Robinson JS, Klionsky DJ, Banta LM, Emr SD. 1988. Protein sorting in
797 Saccharomyces cerevisiae: isolation of mutants defective in the
798 delivery and processing of multiple vacuolar hydrolases. Molecular and
799 Cellular Biology **8**:4936–4948. DOI:
800 https://doi.org/10.1128/mcb.8.11.4936-4948.1988, PMID: 3062374
801 Roelants FM, Breslow DK, Muir A, Weissman JS, Thorner J. 2011. Protein
802 kinase Ypk1 phosphorylates regulatory proteins Orm1 and Orm2 to

control sphingolipid homeostasis in *Saccharomyces cerevisiae*. Proceedings of the National Academy of Sciences **108**:19222–19227. DOI: https://doi.org/10.1073/pnas.1116948108

Romanauska A, Köhler A. 2021. Reprogrammed lipid metabolism protects inner nuclear membrane against unsaturated fat. Developmental Cell **56**:2562-2578.e3. DOI: https://doi.org/10.1016/j.devcel.2021.07.018

Sakai J, Duncan EA, Rawson RB, Hua X, Brown MS, Goldstein JL. 1996. Sterol-Regulated Release of SREBP-2 from Cell Membranes Requires Two Sequential Cleavages, One Within a Transmembrane Segment. Cell **85**:1037–1046. DOI: https://doi.org/10.1016/S0092-8674(00)81304-5

Sakai J, Rawson RB, Espenshade PJ, Cheng D, Seegmiller AC, Goldstein JL, Brown MS. 1998. Molecular Identification of the Sterol-Regulated Luminal Protease that Cleaves SREBPs and Controls Lipid Composition of Animal Cells. Molecular Cell **2**:505–514. DOI: https://doi.org/10.1016/S1097-2765(00)80150-1

Siggers T, Reddy J, Barron B, Bulyk ML. 2014. Diversification of Transcription Factor Paralogs via Noncanonical Modularity in C2H2 Zinc Finger DNA Binding. Molecular Cell **55**:640–648. DOI: https://doi.org/10.1016/j.molcel.2014.06.019

Sikorski RS, Hieter P. 1989. A System of Shuttle Vectors and Yeast Host Strains Designed for Efficient Manipulation of DNA in Saccharomyces ceratisiae. Genetics **122**:19–27.

Stathopoulos AM, Cyert MS. 1997. Calcineurin acts through the *CRZ1/TCN1* -encoded transcription factor to regulate gene expression in yeast. Genes & Development **11**:3432–3444. DOI: https://doi.org/10.1101/gad.11.24.3432

Tabuchi M, Audhya A, Parsons AB, Boone C, Emr SD. 2006. The Phosphatidylinositol 4,5-Biphosphate and TORC2 Binding Proteins Slm1 and Slm2 Function in Sphingolipid Regulation. Molecular and Cellular Biology **26**:5861–5875. DOI: https://doi.org/10.1128/MCB.02403-05

van Meer G, Voelker DR, Feigenson GW. 2008. Membrane lipids: where they are and how they behave. Nature reviews. Molecular cell biology **9**:112–124. DOI: https://doi.org/10.1038/nrm2330, PMID: 18216768

Wang X, Sato R, Brown MS, Hua X, Goldstein JL. 1994. SREBP-1, a membrane-bound transcription factor released by sterol-regulated proteolysis. Cell **77**:53–62. DOI: https://doi.org/10.1016/0092-8674(94)90234-8

White MJ, Hirsch JP, Henry SA. 1991. The *OPI1* gene of Saccharomyces cerevisiae, a negative regulator of phospholipid biosynthesis, encodes a protein containing polyglutamine tracts and a leucine zipper. Journal of Biological Chemistry **266**:863–872. DOI: https://doi.org/10.1016/S0021-9258(17)35253-5

Yamaguchi Y, Katsuki Y, Tanaka S, Kawaguchi R, Denda H, Ikeda T, Funato K, Tani M. 2018. Protective role of the HOG pathway against the growth defect caused by impaired biosynthesis of complex sphingolipids in yeast *Saccharomyces cerevisiae*. Molecular Microbiology **107**:363–386. DOI: https://doi.org/10.1111/mmi.13886

852 Yang H, Tong J, Lee CW, Ha S, Eom SH, Im YJ. 2015. Structural mechanism
853 of ergosterol regulation by fungal sterol transcription factor Upc2.
854 Nature Communications **6**:6129. DOI:
855 https://doi.org/10.1038/ncomms7129
856
857

858 Table 1. Multi-copy suppressor for *lip1-1*-myriocin sensitivity (*MLM* genes)

Suppressor	Number of clones isolated	Gene	Description*
MLM1	8	*LIP1*	Ceramide synthase subunit
MLM2	7	*COM2*	Transcriptional factor that binds IME1 Upstream Activation Signal (UAS)ru
MLM3	2	*TIF3*	Transcription initiation factor eIF-4B
MLM4	2	*YLR149C-A*	Dubious open reading frame
		STM1	Protein required for optimal translation under nutrient stress
MLM5	1	*YPK1*	Ser/Thr protein kinase
MLM6	1	*LSP1*	Eisosome core component
MLM7	1	*BMH2*	14-3-3 protein
MLM8	1	*RIM20*	Protein involved in proteolytic activation of Rim101p
		CAF20	Phosphoprotein of the mRNA cap-binding complex
		YOR277C	Dubious open reading frame; almost completely overlaps the verified gene CAF20
		SNR31	H/ACA box small nuclear RNA (snoRNA)
		SNR5	H/ACA box small nuclear RNA (snoRNA)
		HEM4	Uroporphyrinogen III synthase
		RFM1	Component of the Sum1p-Rfm1p-Hst1p complex
MLM9	1	*MOT3*	Transcriptional repressor, activator
		TVP18	Integral membrane protein
		ABF2	Mitochondrial DNA-binding protein
MLM10	1	*SRO77*	Protein with roles in exocytosis and cation homeostasis
		PKC1	Ser/Thr protein kinase
MLM11	1	*PIN4*	Protein involved in G2/M phase progression and response to DNA damage
		SEC17	Alpha-SNAP cochaperone
MLM12	1	*SUT2*	Zn2Cys6 family transcription factor

859 **Saccharomyces* GENOME DATABSE: https://www.yeastgenome.org/

860

861

862

863

Table 2. Strains used in this study

Strain*	Genotype	Reference or source
Escherichia coli		
JM109	*endA1 glnV44 thi-1 relA1 gyrA96 recA1 mcrB*$^{+}$ Δ(*lac-pro*AB) *e14*$^{-}$ [*F' traD36 proAB*$^{+}$ *lacI*^{q} *lacZΔM15*] *hsdR17*(r_K^{-} m_K^{+})	Laboratory stock
DH5α	*F*$^{-}$ *endA1 glnV44 thi-1 recA1 relA1 gyrA96 deoR nupG Φ80dlacZΔM15 Δ*(*lacZYA-argF*)*U169, hsdR17*(r_K^{-} m_K^{+}), λ^{-}	Laboratory stock
Saccharomyces cerevisiae		
SEY6210	*MATα leu2-3, 112 ura3-52 his3-Δ200 trp1-Δ901 lys2-801 suc2-Δ9*	(Robinson et al., 1988)
SEY6210. 1	*MATa leu2-3, 112 ura3-52 his3-Δ200 trp1-Δ901 lys2-801 suc2-Δ9*	(Robinson et al., 1988)
BY4741	*MAT*a *his3Δ1 leu2Δ0 met15Δ0 ura3Δ0*	Research Genetics
BY4742	*MATα his3Δ1 leu2Δ0 met15Δ0 ura3Δ0*	Research Genetics
BY4743	BY4741×BY4743	Research Genetics
MTY1000	SEY6210; *HIS3MX6:P*$_{\text{tet-off}}$-GFP-*COM2*	This study
MTY1009	SEY6210; *COM2*-13Myc:*HIS3MX6*	This study
MTY1026	SEY6210 *ypk1*Δ::*HIS3MX6 ypk2*Δ::HIS3MX6 carrying pRS415-*YPK1*^{WT} *COM2*-13MYC:*HIS3MX6*	This study
MTY1049	SEY6210 *ypk1Δ::HIS3MX6 ypk2Δ::HIS3MX6 COM2-13MYC:HIS3MX6 carrying pRS415-YPK1*^{L424A}	This study
MTY1061	SEY6210; *HIS3MX6*:*P*$_{\text{tet-off}}$-13Myc-*COM2*	This study
MTY1087	SEY6210; P_{YPK1}-ΔCBS	This study
MTY1192	SEY6210; *tor2Δ::HIS3* carrying pRS415-*tor2-21 COM2*-13Myc:: *HIS3MX6*	This study
MTY1194	SEY6210; *ypk1*^{ts}::*HIS3 ypk2*Δ::*HIS3MX6 COM2*-13Myc:: *HIS3MX6*	This study
MTY1198	SEY6210.1; *slm1*Δ::*HIS3MX6 slm2*Δ::*HIS3MX6 COM2*-13Myc::*HIS3MX6* carrying pRS415-*slm1-1*	This study
MTY1208	SEY6210; *HIS3MX6*::P_{LCB1}-*ΔCBS-LCB1*	This study
MTY1214	SEY6210; P_{YPK1}-*ΔCBS-YPK1 HIS3MX6*::P_{LCB1}-*ΔCBS-LCB1*	This study

MTY1295	SEY6210; *aur1-19 COM2*-13Myc::*HIS3MX6*	This study
DYY1	SEY6210.1; *HIS3MX6:*$P_{tet\text{-}off}$-*lip1-1*	(Ishino et al., 2022)
YIY36	SEY6210; *com2*Δ::*KANMX4*	This study
YIY49	SEY6210.1; *HIS3MX6:*$P_{tet\text{-}off}$-*lip1-1 COM2*-13Myc::*HIS3MX6*	This study
RSY2	SEY6210; *COM2*-13Myc::*HIS3MX6* P_{YPK1}-ΔCBS	This study
KPY28	SEY6210; *pdr5*Δ::*TRP1 COM2*-13Myc::*HIS3MX6*	This study
KPY32	SEY6210; *csg2*Δ::*HIS3 COM2*-13Myc::*HIS3MX6*	This study
KPY34	SEY6210; *ipt1*Δ::*KANMX4 COM2*-13Myc::*HIS3MX6*	This study
*erg1*Δ/*ERG1*	BY4743; *erg1*Δ::*KANMX4/ERG1*	Research Genetics
*ypk1*Δ/*ypk1*Δ	BY4743; *ypk1*Δ::*KANMX4/ypk1*Δ::*KANMX4*	Research Genetics
*com2*Δ/*com2*Δ	BY4743; *com2*Δ::*KANMX4/com2*Δ::*KANMX4*	Research Genetics
*tif3*Δ/*tif3*Δ	BY4743; *tif3*Δ::*KANMX4/tif3*Δ::*KANMX4*	Research Genetics
*stm1*Δ/*stm1*Δ	BY4743; *stm1*Δ::*KANMX4/stm1*Δ::*KANMX4*	Research Genetics
*hog1*Δ/*hog1*Δ	BY4743; *hog1*Δ::*KANMX4/hog1*Δ::*KANMX4*	Research Genetics
*lsp1*Δ/*lsp1*Δ	BY4743; *lsp1*Δ::*KANMX4/lsp1*Δ::*KANMX4*	Research Genetics
*slt2*Δ/*slt2*Δ	BY4743; *slt2*Δ::*KANMX4/slt2*Δ::*KANMX4*	Research Genetics
*ire1*Δ/*ire1*Δ	BY4743; *ire1*Δ::*KANMX4/ire1*Δ::*KANMX4*	Research Genetics

866 Table 3. Plasmids used in this study

Plasmids	Construct	Reference or source
pRS415	*Amp, LEU2*, *CEN6*	(Sikorski and Hieter, 1989)
pRS416	*Amp, URA3*, *CEN6*	(Sikorski and Hieter, 1989)
pRS426	*Amp, URA3, 2 µm*	(Sikorski and Hieter, 1989)
pRT3	pRS416; *URA3, CEN, HIS3MX6-*P_{ADH1}*-tTA2s-*P_{tetoff}*-GFP*	(Ishino et al., 2022)
pMT1447	pRS416; *URA3, CEN*, P_{SNR52}*-YPK1-2-gRNA-*T_{SUP}*-Z4EV-*P_{Z4EV}*-CAS9-CYC1pA*	This study
pMT1536	pRS416; *URA3*, *CEN*, P_{COM2}*-COM2*$^{T251A+S370, 380A}$-13Myc (ST3A)	This study
pMT1547	pRS416; *URA3*, *CEN*, P_{COM2}*-COM2*$^{S88, 164, 370, 380A+T251A}$-13Myc (ST4A)	This study
pMT1576	pRS416; *URA3*, *CEN*, P_{COM2}*-COM2*$^{S88, 164, 235, 370, 380A+T251A}$-13Myc (ST6A)	This study
pMT1577	pRS416; *URA3*, *CEN*, P_{COM2}*-COM2*$^{S88, 164, 235, 359, 370, 380A+T251A}$ -13Myc (ST7A)	This study
pMT1578	pRS416; *URA3*, *CEN*, P_{COM2}*-COM2*$^{S88, 164, 235, 359, 370, 380A+T251, 368A}$ -13Myc (ST8A)	This study
pMT1790	pRS416; *URA3*, *CEN*, P_{COM2}*-COM2*$^{S11, 88, 138, 164, 235, 359, 370, 380A+T251, 368A}$-13Myc (ST10A)	This study
pYI41	yEP352 Suppressor #6 (*YPK1*)	This study
pYI42	yEP352 Suppressor #13 (*TIF3*)	This study
pYI44	yEP352 Suppressor #26 (*RIM20* (partial), *CAF20, HEM4, RFM1*)	This study
pYI46	yEP352 Suppressor #34 (*COM2*)	This study
pYI47	yEP352 Suppressor #36 (*SPO77* (partial), *PKC1* (partial))	This study
pYI48	yEP352 Suppressor #21 (*COM2*)	This study
pYI51	yEP352 Suppressor #9 (*LSP1*)	This study
pYI53	yEP352 Suppressor #176 (*BMH2*)	This study
pYI56	yEP352 Suppressor #56 (*PIN4*)	This study
pYI58	yEP352 Suppressor #66 (*SUT2*)	This study
pYI62	pRS416; P_{COM2}*-COM2*-13Myc (*COM2* WT)	This study
pYI68	pP_{YPK1}*-LacZ*	This study
pAMS366	*Amp, URA3, 4×CDRE-LacZ*	(Stathopoulos and Cyert, 1997)

pRS16	p$P_{YPK1\text{-}\Delta CBS}$ *-LacZ*	This study
pRS18	pP_{LCB1}*-LacZ*	This study
pRS28	p$P_{LCB1\text{-}\Delta CBS}$ *-LacZ*	This study
pNK18	pRS416; *URA3, CEN,* P_{YPK1}*-3HA-YPK1::HIS3MX6*	This study
pNK19	pRS416; *URA3, CEN,* P_{YPK1}*-ΔCom2 binding site (ΔCBS)-3HA-YPK1::HIS3MX6*	This study
pTU3	pRS416; P_{COM2} (-500 to -252)-*COM2*-13Myc	This study
pTU4	pRS416; P_{COM2} (-500 to -115)-*COM2*-13Myc	This study
pTU6	pRS416; P_{COM2} (-500 to -70)-*COM2*-13Myc	This study
pTU14	pRS416; P_{COM2}-*COM2* (Δ2-89)-13Myc	This study
pTU15	pRS416; P_{COM2}-*COM2* (Δ2-190)-13Myc	This study
pTU17	pRS416; P_{COM2} (-500 to -180)-*COM2*-13Myc	This study
pTU28	pRS416; P_{COM2}-*COM2* (Δ380-443)-13Myc	This study
pTU29	pRS416; P_{COM2}-*COM2* (Δ231-443)-13Myc	This study
pTU30	pRS416; P_{COM2}-*COM2* (Δ88-443)-13Myc	This study
pTU33	pRS416; P_{COM2}-*COM2* (Δ2-40)-13Myc	This study
pTU34	pRS416; P_{COM2}-*COM2* (Δ144-443)-13Myc	This study
pKP6	pRS416; P_{COM2}-*COM2* (Δ2-10)-13Myc	This study
pKP7	pRS416; P_{COM2}-*COM2* (Δ2-20)-13Myc	This study
pKP8	pRS416; P_{COM2}-*COM2* (Δ2-30)-13Myc	This study
pKP13	pRS416; P_{COM2}-*COM2* (Δ2-114)-13Myc	This study
pKP14	pRS416; P_{COM2}-*COM2* (Δ2-139)-13Myc	This study
pKP15	pRS416; P_{COM2}-*COM2* (Δ2-164)-13Myc	This study
pKP20	pRS416; P_{COM2}-*COM2* (Δ240-443)-13Myc	This study
pKP21	pRS416; P_{COM2}-*COM2* (Δ290-443)-13Myc	This study
pKP22	pRS416; P_{COM2}-*COM2* (Δ340-443)-13Myc	This study
pKP23	pRS416; P_{COM2}-*COM2* (Δ390-443)-13Myc	This study
pAN28	pRS416; P_{COM2}-*COM2*^{K23,35R}-13Myc	This study
pAN30	pRS416; P_{COM2}-*COM2*^{K23,35,51R}-13Myc	This study
pAN36	pRS416; P_{COM2}-*COM2*^{K51R}-13Myc	This study

867

868

869

870 Table 4. Key resources table

Reagent type (species) or resorce	Designations	Source or reference	Identifiers	Additional information
Antibody	Anti-Com2 (Rabbit polyclonal)	This study	Home made	WB (1:2,000)
Antibody	Anti-Myc (Mouse monoclonal)	Medical & Biological Laboratories Co., Ltd., Nagoya, Japan	Cat # M192-3	WB (1:5,000)
Antibody	Anti-FLAG (Mouse monoclonal)	Sigma-Aldrich, Merck KGaA, Darmstadt, Germany	Cat # F1804	WB (1:2,000)
Antibody	Anti-Ypk1 (Rabbit polyclonal)	(Ishino et al., 2022)	Home made	WB (1:2,000)
Antibody	Anti-phospho-Ypk2^{T659} (Rabbit polyclonal) for detection of both p-Ypk1^{T662} and p-Ypk2	(Ishino et al., 2022)	MBL, Nagoya, Japan; custom-made	WB (1:50,000)
Antibody	Anti-G6PDH (Rabbit polyclonal)	Sigma-Aldrich, Merck KGaA, Darmstadt, Germany	Cat # SAB2100871	WB (1:50,000)
Antibody	Anti-mouse IgG (HRP-conjugated)	Cell Signaling Technology, Danvers, MA, USA	Cat # 7076	WB (1:10,000)
Antibody	Anti-rabbit IgG (HRP-conjugated)	Capel, MP Biomedicals, Solon, OH, USA	Cat # 55611	WB (1:10,000)
Enzyme	KOD -Plus- Neo polymerase	TOYOBO, Co., Ltd., Osaka, Japan	Cat # KOD-401	
Enzyme	PrimeSTAR® GXL polymerase	TaKaRa Bio, Shiga, Japan	Cat # R050A	
Enzyme	Taq DNA polymerase	BioAcademia, Osaka, Japan	Cat # 02-012	
Chemical compound	Myriocin	Sigma-Aldrich, Merck KGaA, Darmstadt, Germany	Cat # M1177	
Chemical compound	Aureobasidin A	TaKaRa Bio, Shiga, Japan	Cat # 630499	
Chemical compound	Doxycycline Hyclate	Tokyo Chemical Industry Co., Ltd., Tokyo, Japan	Cat # D4116	
Chemical compound	Miconazol	FUJIFILM Wako Pure Chemical Corporation, Osaka, Japan	Cat # 510-22771	
Chemical compound	Telbinafine	FUJIFILM Wako Pure Chemical Corporation, Osaka, Japan	Cat # 516-40951	
Chemical compound	Tunicamycin	FUJIFILM Wako Pure Chemical	Cat # 202-08241	

		Corporation, Osaka, Japan		
Chemical compound	Fluorescent Brightener 28 (Calcofluor White)	FUJIFILM Wako Pure Chemical Corporation, Osaka, Japan	Cat # 593-28141	
Chemical compound	1-(tert-butyl)-3-(3-methylbenzyl)-1H-pyrazole[3,4-d] pyrimidin-4-amoine, 3-MB-PP1	Cyman Chemical, Ann Arbor, MI, USA	Cat # 17860	
Software	GraphPad Prism 10	Graphpad Software, San Diego, CA, USA		10.5.0
Software	Adobe Photoshop 2024	Adobe Inc., San Jose, CA, USA		25.3.1
Software	Adobe Illustrator 2024	Adobe Inc., San Jose, CA, USA		28.7.10
Software	Microsoft Excel 365	Microsoft corporation, Redmond, WA, USA		

873 **Figure legends**

874 **Figure 1.** Screening for novel regulatory factors of sphingolipid metabolism.
875 (**A**) *de novo* sphingolipid biosynthesis pathway in yeast, *Saccharomyces*
876 *cerevisiae*. The pathway and proteins responsible for the synthesis of yeast
877 sphingolipids are shown. IPC, inositol phosphorylceramide; MIPC,
878 mannosylinositol phosphorylceramide; $M(IP)_2C$, mannosyldiinositol
879 phosphorylceramide. Myriocin (Myr) and aureobasidin A (AbA) inhibit the
880 indicated steps of the sphingolipid biosynthesis pathway. (**B**) Schematic
881 representation of screening for novel regulatory factors of sphingolipid
882 metabolism by using the Myr-sensitive phenotype of *lip1-1* cells. (**C**) Schematic
883 representation of the TORC2-Ypk1-dependent regulatory mechanism of
884 sphingolipid biosynthesis. (**D**) Wild-type and *lip1-1* cells carrying an indicated
885 plasmid were spotted at a 10-fold serial dilution on YPD supplemented with (0.2
886 μM) or without Myr, in the presence (20 μg/mL) or absence of doxycycline
887 (Dox). (**E**) The diploid homozygous knockout cells of *MLM* genes (*ypk1*Δ, *lsp1*Δ,
888 *com2*Δ, *tif3*Δ, and *stm1*Δ) were spotted at a 10-fold serial dilution on YPD
889 supplemented with 1.0 μM Myr. (**F**, **G**) Wild-type (*COM2*-13Myc) and P_{tetoff}-*lip1-*
890 *1* cells were grown to mid-log in SD (+All) liquid medium in the presence (+) or
891 absence (-) of Dox (20 μg/mL) and treated under the respective conditions for
892 3 hrs. Cells were then harvested and total cell lysates were prepared. The
893 lysates were resolved by SDS-PAGE and immunoblotted with anti-Myc or anti-
894 G6PDH antibodies, to detect Com2-13Myc or G6PDH (loading control),
895 respectively. Western blot experiments were independently replicated three
896 times. Values for Com2 expression level are expressed as mean ± SD (n≥3).

897

898 **Figure 1—figure supplement 1.** Screening to identify sphingolipid metabolism
899 related factors that suppress Myriocin sensitivity of *lip1-1* cells. Wild-type cells
900 and *lip1-1* cells carrying a plasmid including each suppresser gene were
901 spotted in 10-fold serial dilution on YPD supplemented with 0.2 μM Myriocin
902 (Myr) in the presence of Dox (20 μg/mL).

903

904

905 **Figure 1—figure supplement 2.** The diploid homozygous knockout cells of
906 *MLM* genes were spotted at a 10-fold serial dilution on YPD supplemented with
907 0, 1.0, 2.0 μM Myr and incubated at 26 ˚C for 2-3 days.
908
909 **Figure 1—figure supplement 3.** (**A**) Wild-type, *ypk1*Δ, *com2*Δ, *hog1*Δ, *slt2*Δ
910 and *ire1*Δ cells were spotted in 10-fold serial dilution on YPD for each condition
911 (26 ˚C, 37 ˚C, 75 mM Acetic acid (AcOH), 50 mM Tris-HCl pH 8.0, 1 M NaCl,
912 0.25 μg/mL Tunicamycin (TN), 20 μg/mL Calcofluor white (CFW), 0.0150%
913 SDS, 50 ng/mL Miconazole, 0.6 μM / 1.0 μM Myr, and 75 ng/mL AbA. (**B**)
914 Detailed description of each step of the *de novo* sterol biosynthetic pathway in
915 the yeast *Saccharomyces cerevisiae* and its experimental mechanism of action.
916 The pathway and proteins responsible for the synthesis of yeast sterols are
917 shown. (**C**) The indicated cells were spotted in 10-fold serial dilutions onto YPD
918 supplemented with 10 μM, 50 μM, and 100 μM Terbinafine. (**E**, **F**) Wild-type
919 cells were grown to mid-log phase in SD liquid medium and separately treated
920 with 1.0 μM Myr, 50 μM Terbinafine, or 50 ng/ml Miconazole for 3 hrs at 26 ˚C,
921 after which lysates were separated by SDS-PAGE and immunoblotted with anti-
922 Myc or anti-G6PDH antibodies to detect Com2-13Myc or G6PDH (loading
923 control), respectively. The amount of Com2-13Myc in wild-type cells (without
924 Myr) was normalized to the amount of G6PDH, and each data was set as 100%.
925 Data represents the mean ± SD of three independent experiments. Statistical
926 significance was determined by one-way ANOVA followed by Tukey's multiple
927 comparison test (****p<0.0001, ns: not significant).
928
929 **Figure 2.** Com2 functions upstream of the TORC2-Ypk1 pathway. (**A**)
930 Schematic representation of Com2, with the positions of the predicted AGC-
931 kinase-dependent phosphorylation sites and two Zinc-finger domains
932 highlighted. (**B**) Characterization of *ypk1-as ypk2*Δ mutant. Wild-type, the ATP-
933 analogue sensitive allele *ypk1*^{L424A}, *ypk1-as ypk2*Δ cells and the wild-type allele
934 of Ypk1, *YPK1*^{WT} *ypk2*Δ cells were spotted on YPD containing DMSO (Mock)
935 or indicated concentration of 3MB-PP1 and incubated for 3 days at 26 ˚C. *ypk1-*
936 *as ypk2*Δ cells exhibit growth defect by limiting of Ypk1-activity by addition of
937 3MB-PP1. (**C**) Wild-type cells, *YPK1*^{WT} *ypk2*Δ cells and *ypk1-as ypk2*Δ cells are

938 spotted on YPD and YPD containing 0.7 μM myriocin and incubated for 2 days
939 at 26 ˚C. *ypk1-as ypk2*Δ cells exhibit Myr-sensitive without inhibition by addition
940 of 3MB-PP1. (**D**) Wild-type *YPK1*^{WT} *ypk2*Δ cells and analogue-sensitive mutant
941 *YPK1*^{L424A}*ypk2*Δ cells carrying the plasmid expressing Com2-13Myc were
942 treated with 3MB-PP1 for the indicated time-periods and then treated with 1.0
943 μM Myr for 2 hrs. The lysates were then resolved using phos-tag or normal
944 SDS-PAGE and immunoblotted with anti-Myc, anti-FLAG, or anti-G6PDH
945 antibodies, to detect Com2-13Myc, 3FLAG-Lag1, or G6PDH (loading control),
946 respectively. (**E**) Wild-type (BY4743) and knockout homozygote diploid cells of
947 *ypk1*Δ or *com2*Δ carrying an indicated multi-copy plasmid were spotted at a 10-
948 fold serial dilution on YPD supplemented with the indicated concentrations of
949 Myr.
950
951 **Figure 3.** Ypk1 is expressed in a Com2-dependent manner. (**A**) Proposed
952 model for the mechanism by which sphingolipid depletion increases Com2
953 expression, induces *YPK*1 transcription, and activates the TORC2-Ypk1
954 pathway to promote sphingolipid biosynthesis. (**B**) Wild-type and *com2*Δ cells
955 were grown to mid-log phase in SD liquid medium and then treated with 1.0 μM
956 Myr. The cells were then harvested, and total cell lysates were prepared from
957 them. The lysates were resolved using SDS-PAGE and immunoblotted with
958 anti-Myc, anti-Ypk1, anti-phospho-Ypk1^{T662}, or anti-G6PDH antibodies, to
959 detect Com2-13Myc, Ypk1, TORC2-dependent phosphorylation site
960 (hydrophobic motif) of Ypk1 (p-Ypk1^{T662}) or G6PDH (loading control),
961 respectively. (**C**) The time-dependent increase in Com2 expression following
962 Myr treatment was quantified in wild-type cells. Experiments were performed
963 three times independently. Com2 levels were normalized to the internal control
964 G6PDH, with the value at 0 min of Myr treatment set to 1. Data are presented
965 as the mean ± SD from three independent experiments. Asterisks indicate
966 statistically significant differences compared with the 0 min time point as
967 determined by one-way ANOVA followed by Tukey's multiple comparisons test
968 (****p<0.0001). (**D, E**) To examine time-dependent changes in Ypk1 or
969 phosphorylated Ypk1 at T662 (p-Ypk1^{T662}) in wild-type and *com2*Δ cells, the
970 levels of Ypk1 or p-Ypk1^{T662} at each time point after Myr treatment were

971 normalized to the loading control G6PDH and then further normalized to the
972 value at 0 min before Myr treatment in wild-type cells (set to 1). Data are
973 presented as the mean ± SD from three independent experiments. Asterisks
974 indicate statistically significant differences as determined by two-way ANOVA
975 followed by Sidak's multiple comparisons test (**p<0.01, ***p<0.001,
976 ****p<0.0001). (**F**) To examine time-dependent changes in phosphorylated
977 Ypk1 at T662 (p-Ypk1^{T662}) in wild-type and *com2*Δ cells, the levels of p-Ypk1^{T662}
978 at each time point after Myr treatment were normalized to total Ypk1 and then
979 further normalized to the value at 0 min before Myr treatment in wild-type cells
980 (set to 1). Data are presented as the mean ± SD from three independent
981 experiments. Asterisks indicate statistically significant differences as
982 determined by two-way ANOVA followed by Sidak's multiple comparisons test
983 (**p=0.0092). (**G**) Wild-type, *slm1*^{ts}*slm2*Δ, *tor2*^{ts}, and *ypk1*^{ts}*ypk2*Δ cells were
984 grown to mid-log phase in SD liquid medium at 26°C and then shifted to 37°C
985 for 30 min and treated with 1.0 μM Myr. The cells were then harvested at the
986 indicated time-point and total cell lysates were prepared from them. The lysates
987 were resolved using SDS-PAGE and immunoblotted with anti-Ypk1, anti-Myc,
988 anti-G6PDH antibodies, or anti-phospho-Ypk1^{T662} antibodies, to detect Ypk1,
989 Com2-13Myc, G6PDH (loading control), or TORC2-dependent phosphorylation
990 of Ypk1 (p-Ypk1^{T662}), respectively.
991
992 **Figure 4.** Overexpression of Com2 causes increased expression of Ypk1. (**A**)
993 The chromosomal *COM2* promoter (P_{COM2}) was replaced by a Tet-off promoter
994 and GFP was fused to the N-terminus of Com2, to generate the $P_{tet\text{-}off}$-GFP-
995 *COM2* strain. (**B**) Wild-type, *com2*Δ, and $P_{tet\text{-}off}$-GFP-*COM2* cells were spotted
996 at a 10-fold serial dilution on YPD supplemented with 0.6 or 1.0 μM Myr, in the
997 presence (20 μg/mL) (+) or absence (-) of Dox. (**C**) *YPK1* and *LCB1* possess a
998 putative Com2-binding site (CBS) in the promoter region. *LacZ* reporter
999 plasmids containing the wild-type or Com2-binding site (CBS)-deleted promoter
1000 regions of *YPK1* or *LCB1* were used to assess Com2-dependent transcriptional
1001 regulation. (**D**) $P_{tet\text{-}off}$-*GFP-COM2* cells were grown to mid-log phase in SD liquid
1002 medium in the presence (+) or absence (−) of doxycycline (Dox) and then
1003 treated with 1.0 μM Myr for 2 hrs. Cell lysates were subjected to SDS-PAGE

1004 followed by immunoblotting with anti-Com2, anti-Ypk1, anti-Myc, or anti-
1005 G6PDH antibodies to detect GFP-Com2, Ypk1, Lcb1-13Myc, or G6PDH
1006 (loading control), respectively. A representative immunoblot is shown. The full
1007 set of immunoblots from six independent experiments is provided in Figure 4—
1008 figure supplement 2. (**E**) Quantification of Ypk1 and Lcb1 protein levels shown
1009 in Figure 4—figure supplement 2. Band intensities were quantified using
1010 ImageJ. Data are presented as the mean ± SD from six independent
1011 experiments. Statistical significance was assessed using paired t-test (Ypk1,
1012 p=0.0071; Lcb1, p=0.0151). The right panel indicates paired differences with
1013 mean difference and 95% confidence intervals. (**F**) $P_{\text{tet-off}}$-GFP-*COM2* cells
1014 carrying pP_{YPK1}-*LacZ*, p$P_{YPK1CBS\Delta}$-*LacZ* or pP_{LCB1}-*LacZ*, p$P_{LCB1CBS\Delta}$-*LacZ*
1015 plasmid were grown to mid-log phase in SD liquid medium, in the presence (+)
1016 or absence (-) of Dox. Lysates were obtained from the indicated samples and
1017 assayed for β-galactosidase activity. Data are presented as the mean ± SD
1018 from three independent experiments. ***p<0.001, as assessed using one-way
1019 ANOVA, with Tukey multiple comparison tests.
1020
1021 **Figure 4—figure supplement 1.** *In silico* analysis to identify the candidate
1022 genes of the Com2 dependent expression in response to reduced
1023 sphingolipids. Schematic representation of the workflow for the bioinformatic
1024 approach towards identifying Com2 targets from the *S. cerevisiae* genome
1025 using Yeast Genome Pattern Matching (https://www.yeastgenome.org/nph-
1026 patmatch).
1027
1028 **Figure 4—figure supplement 2.** Raw immunoblot data used for the
1029 quantification shown in Figure 4E. $P_{\text{tet-off}}$-*GFP-COM2* cells were grown to mid-
1030 log phase in SD liquid medium in the presence (+) or absence (−) of doxycycline
1031 (Dox) and then treated with 1.0 μM Myr for 2 hrs. Cell lysates from six
1032 independent experiments were subjected to SDS-PAGE followed by
1033 immunoblotting with anti-Ypk1, anti-Myc, or anti-G6PDH antibodies to detect
1034 Ypk1, Lcb1-13Myc, or G6PDH (loading control), respectively.
1035

1036 **Figure 5.** The Com2-binding site in the *YPK1* promoter is required for both
1037 proper expression and TORC2-dependent phosphorylation of Ypk1. (**A**) A
1038 schematic representation of the generation of the P_{YPK1}-Com2 binding site–
1039 deleted (P_{YPK1}-Δ*CBS*) strain using CRISPR-Cas9-mediated genome editing.
1040 The Cas9-gRNA complex introduces a double-strand break near the putative
1041 Com2 binding site (CBS) in the chromosomal *YPK1* promoter (P_{YPK1}). A donor
1042 DNA fragment lacking the CBS (P_{YPK1}ΔCBS) is simultaneously introduced and
1043 integrated into the chromosome by homologous recombination, resulting in
1044 deletion of the CBS from the endogenous *YPK1* promoter. (**B**) Wild-type,
1045 *com2*Δ, and P_{YPK1}-*CBS*Δ cells were spotted at a 10-fold serial dilution on YPD
1046 supplemented with or without 0.6 μM Myr. (**C**) Wild-type, *com2*Δ, P_{YPK1}Δ*CBS*,
1047 and $P_{tet\text{-}off}$-GFP-*COM2* cells were grown to the exponential phase, diluted to
1048 OD_{600}=0.1, and grown in YPD liquid medium treated with or without 0.6 μM Myr,
1049 in the absence (-) or presence (+) of Dox (20 μg/mL), in a microtiter plate. (**D,**
1050 **E, F, G**) The indicated cells were grown to mid-log phase in SD liquid medium
1051 and treated with 1.0 μM Myr at 26°C for 3 hrs. Cells were then harvested and
1052 whole cell lysates were prepared. Whole cell lysates were separated by SDS-
1053 PAGE and immunoblotted with anti-Myc, anti-Ypk1, anti-phospho-Ypk1^{T662} or
1054 anti-G6PDH antibodies to detect Com2-13Myc, Ypk1, p-Ypk1^{T662} or G6PDH
1055 (loading control), respectively. The amounts of Com2-13Myc, Ypk1, and p-
1056 Ypk1^{T662} in wild-type cells (containing Myr) were normalized by the amount of
1057 G6PDH. Data represents the mean ± SD of three independent experiments.
1058 Statistical significance was determined by one-way ANOVA followed by
1059 Tukey's multiple comparison test (*p<0.05, **p<0.01, ns: no significant
1060 difference). (**H**) TLC analysis of sphingolipids extracted from wild-type, *com2*Δ,
1061 P_{YPK1}-*CBS*Δ, and $P_{tet\text{-}off}$-GFP-*COM2* cells. Cells were grown to mid-log phase
1062 in YPD liquid medium, in the presence (+) or absence (-) of Dox (20 μg/mL) and
1063 treated with or without 0.2 μM Myr for 3 hrs. Complex sphingolipids were
1064 analyzed using TLC (left). The level of total complex sphingolipids in the wild-
1065 type cells was taken as 100% and each value is displayed as a graph (right).
1066 The data have been represented as mean ± SD of four independent
1067 experiments. Statistical significance was determined by one-way ANOVA

1068 followed by Tukey's multiple comparison test (*p<0.05, ***p =0.0002, and
1069 ****p<0.0001).
1070
1071 **Figure 5—figure supplement.** Evaluation of myriocin sensitivity in *YPK1* and
1072 *LCB1* promoter CBS-deletion mutants. (**A**) Wild-type, *com2*Δ, P_{YPK1}-Δ*CBS*,
1073 P_{LCB1}-Δ*CBS*, or P_{YPK1}-Δ*CBS*/P_{LCB1}-Δ*CBS* double-mutant strains were spotted
1074 as 10-fold serial dilutions (starting at OD_{600}=1) onto YPD agar plates containing
1075 myriocin (0, 0.6, or 0.8 μM) and incubated at 26°C for 2-3 days to assess
1076 myriocin sensitivity. (**B**) The same strains were cultured in YPD liquid medium
1077 containing myriocin (0 or 0.4 μM) in microplates, and growth curves were
1078 obtained by measuring OD_{600} every 30 min. (**C**) OD_{600nm} values at 20 hrs of
1079 cultivation in the presence of myriocin (0 or 0.4 μM) were quantified (n=3).
1080 Statistical significance was determined by one-way ANOVA followed by
1081 Tukey's multiple comparison test (**p<0.01, ****p<0.0001, ns: no significant
1082 difference).
1083
1084 **Figure 6.** Com2 expression is regulated by sequences within the ORF region.
1085 (**A**) Schematic representation of Com2 expression plasmids carrying stepwise
1086 deletions in the 5′ upstream promoter region or truncations of the Com2 open
1087 reading frame (ORF) from either the N-terminal or C-terminal side. (**B**) The
1088 promoter- or ORF-deletion mutants of Com2 shown in (A) were transformed
1089 into *com2*Δ cells, and functional complementation of the Myr sensitivity of the
1090 *com2*Δ strain was assessed by spot assays using 10-fold serial dilutions on
1091 YPD medium or YPD medium supplemented with 0.6 μM Myr. (**C**) Expression
1092 of Com2-13Myc variants carrying stepwise deletions in the 5′ upstream
1093 promoter region of *COM2* was examined in untreated cells or cells treated with
1094 1.0 μM Myr for 3 hrs. (**D**) Expression of Com2-13Myc variants carrying N-
1095 terminal truncations of the ORF was analyzed under the same conditions as in
1096 (C). (**E**) Expression of Com2-13Myc variants carrying C-terminal truncations of
1097 the ORF was analyzed under the same conditions as in (C). For (C-E), *com2*Δ
1098 cells expressing 13Myc-tagged Com2 wild-type or deletion variants were grown
1099 to mid-log phase in SD (-Ura) liquid medium at 26°C, treated with 1.0 μM Myr
1100 for 3 hrs, and lysed. Proteins were separated by SDS-PAGE and

1101 immunoblotted with anti-Myc, anti-Ypk1, or anti-G6PDH antibodies to detect
1102 Com2-13Myc, Ypk1, or G6PDH (loading control), respectively.
1103
1104 **Figure 6—figure supplement.** Myriocin-dependent upregulation of Com2
1105 expression is independent of the promoter. $P_{tet\text{-}off}$-*13Myc-COM2* cells were
1106 grown to logarithmic phase in SD liquid medium in the presence (+Dox) or
1107 absence (−Dox) of doxycycline. Myriocin was then added to a final
1108 concentration of 1 μM, and protein extracts were prepared at the indicated time
1109 points. The expression levels of 13Myc-Com2 and Ypk1 were analyzed by
1110 immunoblotting. G6PDH was used as a loading control.
1111
1112 **Figure 7.** Com2 is regulated by ubiquitin-proteasome system-mediated
1113 degradation in a manner dependent on intracellular sphingolipid levels. (**A**)
1114 Sphingolipid biosynthetic pathway and perturbations at each step (Myr, PHS
1115 bypass, *lip1-1* +Dox, *aur1-19* +AbA, *csg2*Δ, *ipt1*Δ). (**B**) Immunoblot of Com2
1116 and Ypk1 in wild-type cells treated with 1.0 μM Myr for 3 hrs, followed by 10 μM
1117 PHS for 3 hrs. G6PDH, loading control. (**C-E**) Quantification of (B): Com2 (C),
1118 Ypk1 (D), and p-Ypk1^{T662} (E). One-way ANOVA with Tukey's test. (**F**) PHS-
1119 induced Com2 degradation in wild-type and sphingolipid-pathway-perturbed
1120 cells. Log-phase cultures were pretreated with 1 μM Myr for 3 hrs, then PHS for
1121 3 hrs. *lip1-1* was cultured with Dox (20 μg/mL) from the preculture; *aur1-19* was
1122 pretreated with AbA (20 μg/mL) for 15 min before PHS. Immunoblots for Com2,
1123 Ypk1, and p-Ypk1^{T662}; G6PDH, loading control. (**G**, **H**) Quantification of (F).
1124 Two-way ANOVA with Sidak's test. (**I**) Proteasome inhibition stabilizes
1125 ubiquitinated Com2. Wild-type cells depleted of sphingolipids by Myr (3 hrs)
1126 were incubated ±MG132 (50 μM) and bortezomib (100 μM) for 30 min, followed
1127 by PHS (10 μM). Samples were collected at 0-60 min and immunoblotted with
1128 anti-Myc (Com2-13Myc) and anti-G6PDH. (**J**) Quantification of (I) (normalized
1129 to G6PDH). Two-way ANOVA with Sidak's test. (**K**) Model: Myr stabilizes Com2
1130 to promote *YPK1* expression and sphingolipid biosynthesis, whereas under
1131 +PHS conditions, Com2 is rapidly degraded via the ubiquitin-proteasome
1132 system. Quantified data (C-E, G-H, J) are mean ± SD (n=3). *p<0.1, **p<0.01,
1133 ***p<0.001, ****p<0.0001; n.s., not significant.

1134

1135 **Figure 7—figure supplement.** Wild-type and *atg5*Δ cells expressing Com2-
1136 13Myc were treated with 1.0 μM Myr for 3 hrs., followed by the addition of 10
1137 μM PHS and further incubation for 3 hrs. Samples were collected at the
1138 indicated time points, and Com2-13Myc protein levels were analyzed by
1139 immunoblotting. G6PDH was used as a loading control.

1140

1141 **Figure 8.** Ubiquitination sites required for sphingolipid-dependent proteasomal
1142 degradation of Com2 and the role of Com2 phosphorylation. (**A**) *com2*Δ cells
1143 expressing wild-type Com2 or Com2 (Δ2-40) were treated with 1.0 μM Myr for
1144 3 hrs, then with PHS for 3 hrs; Com2 levels were analyzed by immunoblotting
1145 (G6PDH, loading control). (**B**) Schematic of predicted ubiquitination and
1146 phosphorylation sites in Com2. (**C**) *com2*Δ cells expressing wild-type Com2 or
1147 the indicated lysine mutants (K23,35R, K51R, K23,35,51R) were treated with
1148 1.0 μM Myr for 3 hrs, then 10 μM PHS for 3 hrs; Com2 levels after Myr and after
1149 PHS were analyzed by immunoblotting (G6PDH, loading control). (**D**, **E**)
1150 Immunoblot (D) and quantification (E) comparing wild-type and K23,35,51R
1151 Com2 before and after PHS (n=3; one-way ANOVA with Tukey's test; *p<0.1;
1152 n.s.). (**F**) Com2 phosphorylation was assessed ±λPPase in cells expressing
1153 wild-type Com2 or K23,35,51R after Myr→PHS treatment; immunoblotting for
1154 Com2 (G6PDH, loading control). (**G**) Phos-tag SDS-PAGE of Com2
1155 phosphorylation-site mutants (ST-A3, ST-A5, ST-A7, ST-A8, ST-A10) based on
1156 mobility shifts. (**H**) Immunoblot analysis of Com2 levels in the indicated
1157 phosphorylation-site mutants before and after Myr (3 hrs) → PHS (3 hrs)
1158 treatment (G6PDH, loading control). (**I**, **J**) Immunoblot (I) and quantification (J)
1159 comparing wild-type and ST-A10 Com2 before and after PHS (n=3; one-way
1160 ANOVA with Tukey's test; *p<0.1; n.s.).

1161

1162 **Figure 8—figure supplement.** (**A**) *com2*Δ cells expressing wild-type Com2, an
1163 empty vector, or Com2 mutants carrying substitutions at the predicted
1164 ubiquitination sites were spotted in 10-fold serial dilutions onto YPD medium
1165 containing the indicated concentrations of myriocin (Myr). (**B**) Analysis of
1166 putative phosphorylation sites in Com2. Phosphorylation sites of Com2

1167 annotated in the *Saccharomyces* Genome Database (SGD), putative Ypk1
1168 phosphorylation sites reported by Muir et al., and AGC kinase–dependent
1169 phosphorylation sites in Com2 predicted using the GPS web server
1170 (http://gps.biocuckoo.org/online.php) are shown. Serine/threonine residues
1171 mutated to alanine in the stepwise phosphorylation-site mutants are indicated.
1172 (**C**) Wild-type or *com2*Δ cells transformed with plasmids expressing wild-type
1173 Com2 or the indicated phosphorylation-site mutants were spotted in 10-fold
1174 serial dilutions onto YPD medium containing the indicated concentrations of
1175 Myr.
1176
1177 **Figure 9.** Model for sphingolipid (SL) level-dependent regulation of Com2
1178 degradation via the ubiquitin-proteasome system. When intracellular SL levels
1179 are low, degradation of Com2 is suppressed, allowing Com2 to induce the
1180 expression of its target genes, such as *YPK1* and *LCB1*, which harbor Com2-
1181 binding sites (CBSs) in their promoter regions, thereby promoting sphingolipid
1182 biosynthesis. In contrast, when intracellular SL levels are sufficient, complex
1183 sphingolipids such as MIPC, $M(IP)_2C$ are sensed by an as-yet-unidentified
1184 sphingolipid sensor, leading to phosphorylation of Com2, presumably by an
1185 unidentified kinase. This phosphorylation promotes ubiquitination of Com2 and
1186 its subsequent degradation by the proteasome.

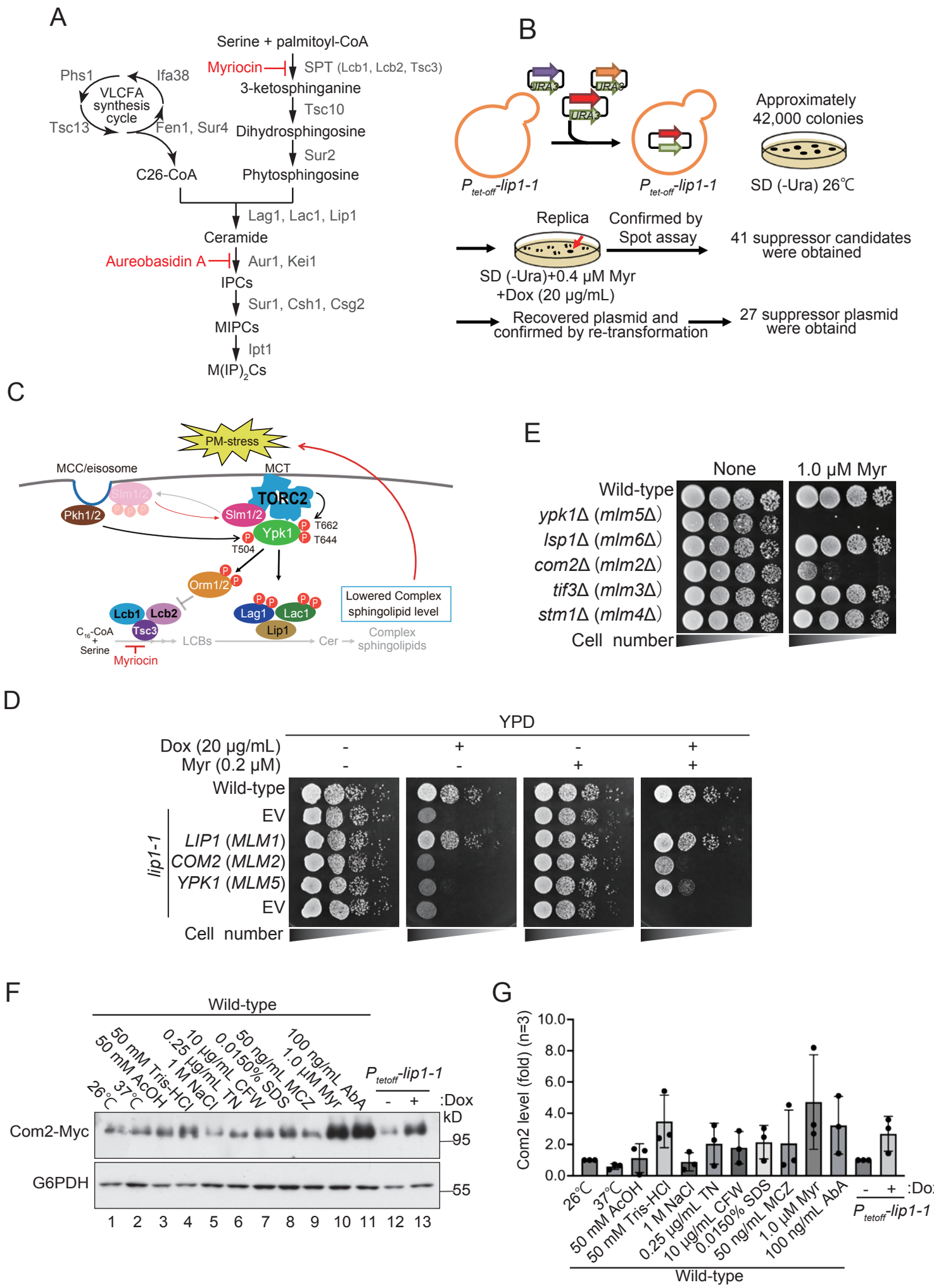
A
Serine + palmitoyl-CoA
Myriocin
SPT (Lcb1, Lcb2, Tsc3)
3-ketosphinganine
Tsc10
Dihydrosphingosine
Sur2
Phytosphingosine
Phs1
Ifa38
VLCFA synthesis cycle
Tsc13
Fen1, Sur4
C26-CoA
Lag1, Lac1, Lip1
Ceramide
Aureobasidin A
Aur1, Kei1
IPCs
Sur1, Csh1, Csg2
MIPCs
Ipt1
M(IP)2Cs
B
URA3
P tet-off-lip1-1
P tet-off-lip1-1
Approximately 42,000 colonies
SD (-Ura) 26℃
Replica
Confirmed by Spot assay
41 suppressor candidates were obtained
SD (-Ura)+0.4 μM Myr +Dox (20 μg/mL)
Recovered plasmid and confirmed by re-transformation
27 suppressor plasmid were obtaind
C
PM-stress
MCC/eisosome
MCT
Pkh1/2
Slm1/2
TORC2
Ypk1
T662
T644
T504
Orm1/2
Lcb1
Lcb2
Tsc3
Lag1
Lac1
Lip1
Lowered Complex sphingolipid level
C16-CoA + Serine
LCBs
Cer
Complex sphingolipids
Myriocin
E
None
1.0 μM Myr
Wild-type
ypk1Δ (mlm5Δ)
lsp1Δ (mlm6Δ)
com2Δ (mlm2Δ)
tif3Δ (mlm3Δ)
stm1Δ (mlm4Δ)
Cell number
D
YPD
Dox (20 μg/mL)
Myr (0.2 μM)
Wild-type
lip1-1
EV
LIP1 (MLM1)
COM2 (MLM2)
YPK1 (MLM5)
EV
Cell number
F
Wild-type
26℃
37℃
50 mM AcOH
50 mM Tris-HCl
1 M NaCl
0.25 μg/mL TN
10 μg/mL CFW
0.0150% SDS
50 ng/mL MCZ
1.0 μM Myr
100 ng/mL AbA
P tetoff-lip1-1
:Dox
kD
Com2-Myc
G6PDH
95
55
1 2 3 4 5 6 7 8 9 10 11 12 13
G
Com2 level (fold) (n=3)
10.0
8.0
6.0
4.0
2.0
0.0
26℃
37℃
50 mM AcOH
50 mM Tris-HCl
1 M NaCl
0.25 μg/mL TN
10 μg/mL CFW
0.0150% SDS
50 ng/mL MCZ
1.0 μM Myr
100 ng/mL AbA
:Dox
P tetoff-lip1-1
Wild-type

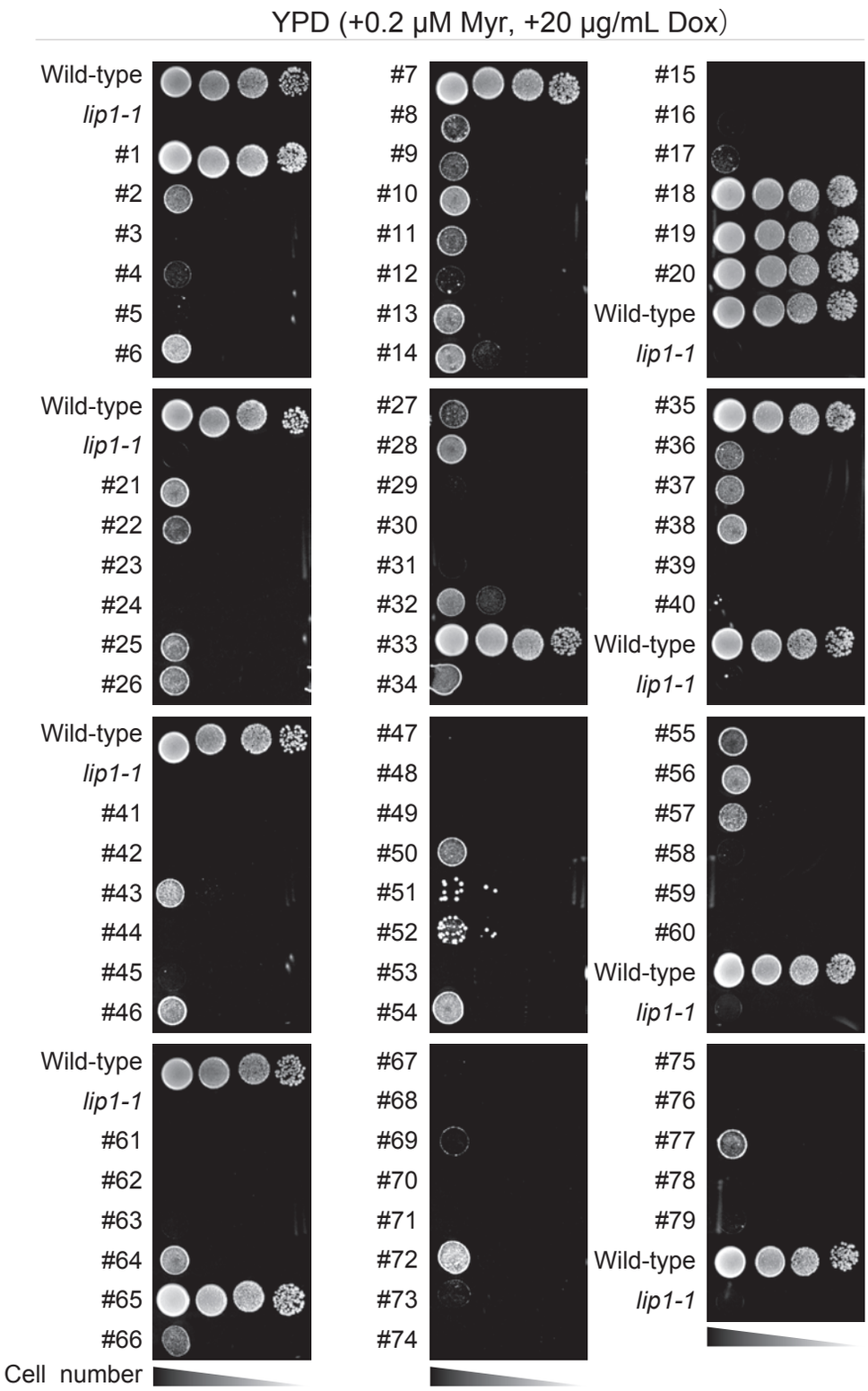

MLM1 (*LIP1*) : #1, #7, #18, #19, #20, #33, #35, #65
MLM2 (*COM2*) : #21, #34, #38, #46, #55, #64, #77
MLM3 (*TIF3*) : #11, #13
MLM4 (*STM1*) : #50, #54
MLM5 (*YPK1*) : #6
MLM6 (*LSP1*) : #9
MLM7 (*BMH2*) : #17
MLM8 (*RIM20* (partial), *CAF20*, *HEM4*, *RFM1*) : #26
MLM9 (*TVP18*): #28
MLM10 (*SRO77* (partial), *PKC1* (partial)): #36
MLM11 (*PIN4*): #56
MLM12 (*SUT2*): #66

Figure 1-figure supplement 1

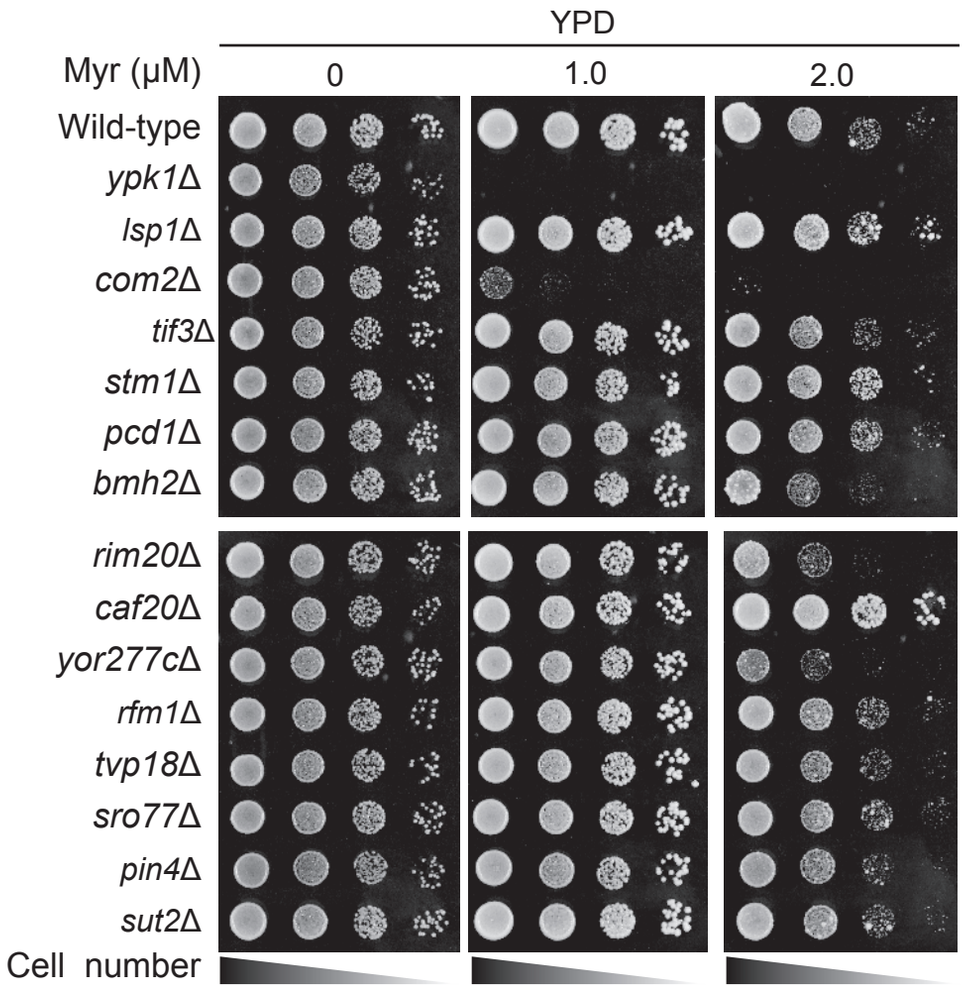

Figure 1-figure supplement 2

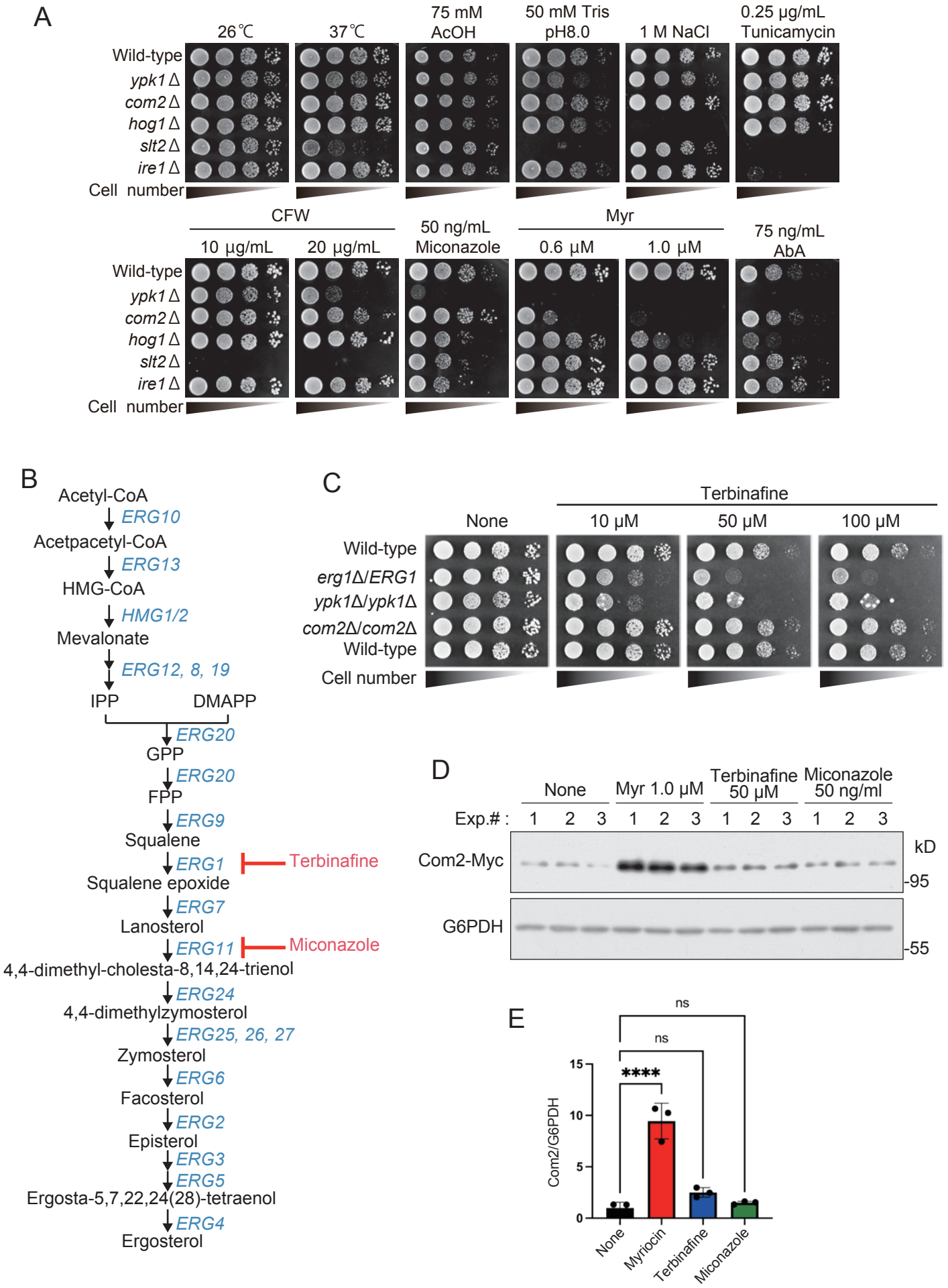

Figure 1-figure supplement 3

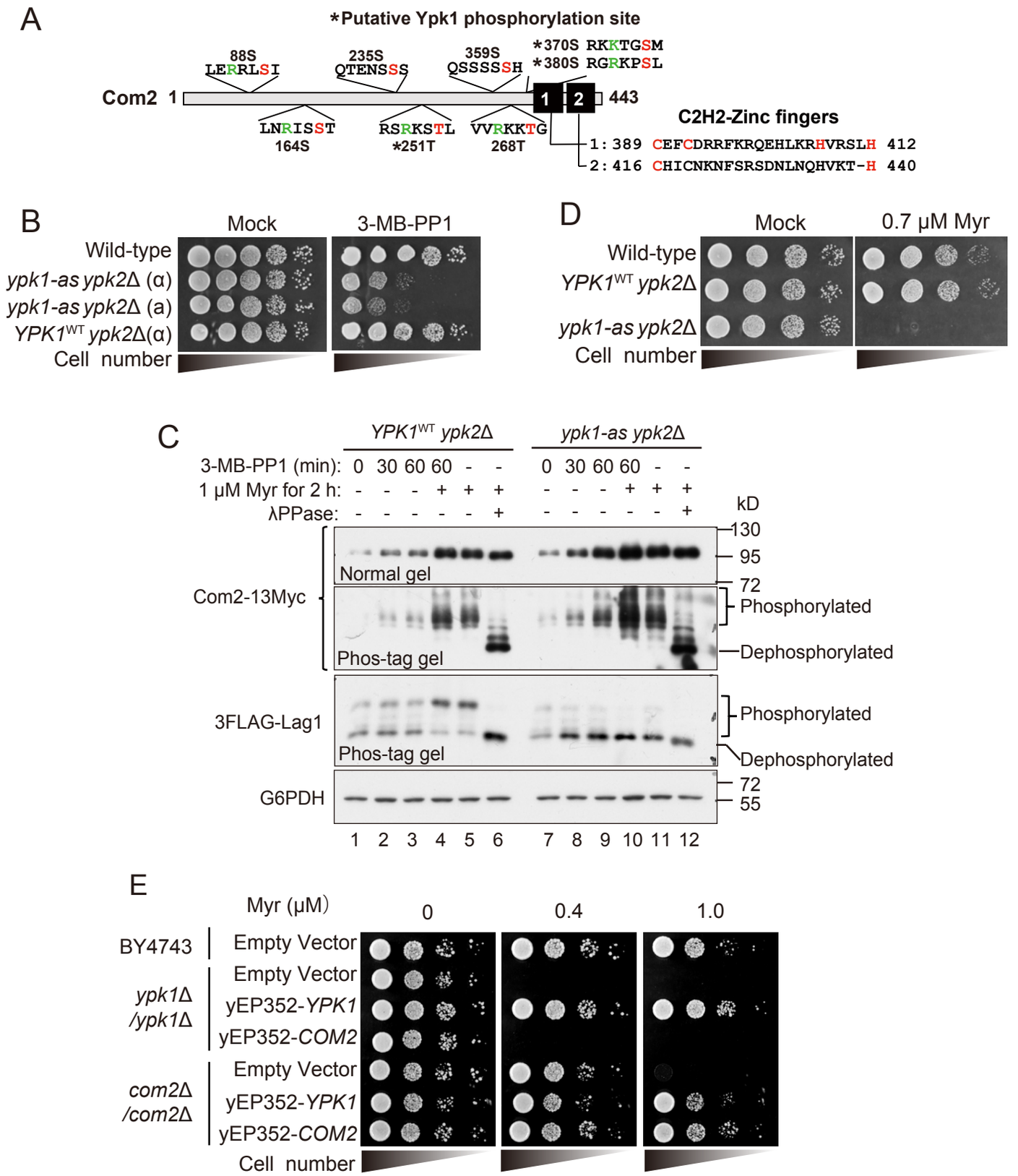
A
*Putative Ypk1 phosphorylation site
88S
LERRLSI
235S
QTENSSS
359S
QSSSSSH
*370S RKKTGSM
*380S RGRKPSL
Com2 1
1
2
443
LNRISST
164S
RSRKSTL
*251T
VVRKKTG
268T
C2H2-Zinc fingers
1: 389 CEFCDRRFKRQEHLKRHVRSLH 412
2: 416 CHICNKNFSRSDNLNQHVKT-H 440
B
Mock
3-MB-PP1
Wild-type
ypk1-as ypk2Δ (α)
ypk1-as ypk2Δ (a)
YPK1WT ypk2Δ(α)
Cell number
D
Mock
0.7 μM Myr
Wild-type
YPK1WT ypk2Δ
ypk1-as ypk2Δ
Cell number
C
YPK1WT ypk2Δ
ypk1-as ypk2Δ
3-MB-PP1 (min): 0 30 60 60 - - 0 30 60 60 - -
1 μM Myr for 2 h: - - - + + + - - - + + +
λPPase: - - - - - + - - - - - +
kD
130
95
72
Com2-13Myc
Normal gel
Phosphorylated
Phos-tag gel
Dephosphorylated
3FLAG-Lag1
Phosphorylated
Phos-tag gel
Dephosphorylated
G6PDH
72
55
1 2 3 4 5 6 7 8 9 10 11 12
E
Myr (μM)
0
0.4
1.0
BY4743
Empty Vector
ypk1Δ /ypk1Δ
Empty Vector
yEP352-YPK1
yEP352-COM2
com2Δ /com2Δ
Empty Vector
yEP352-YPK1
yEP352-COM2
Cell number

Figure 2

! !

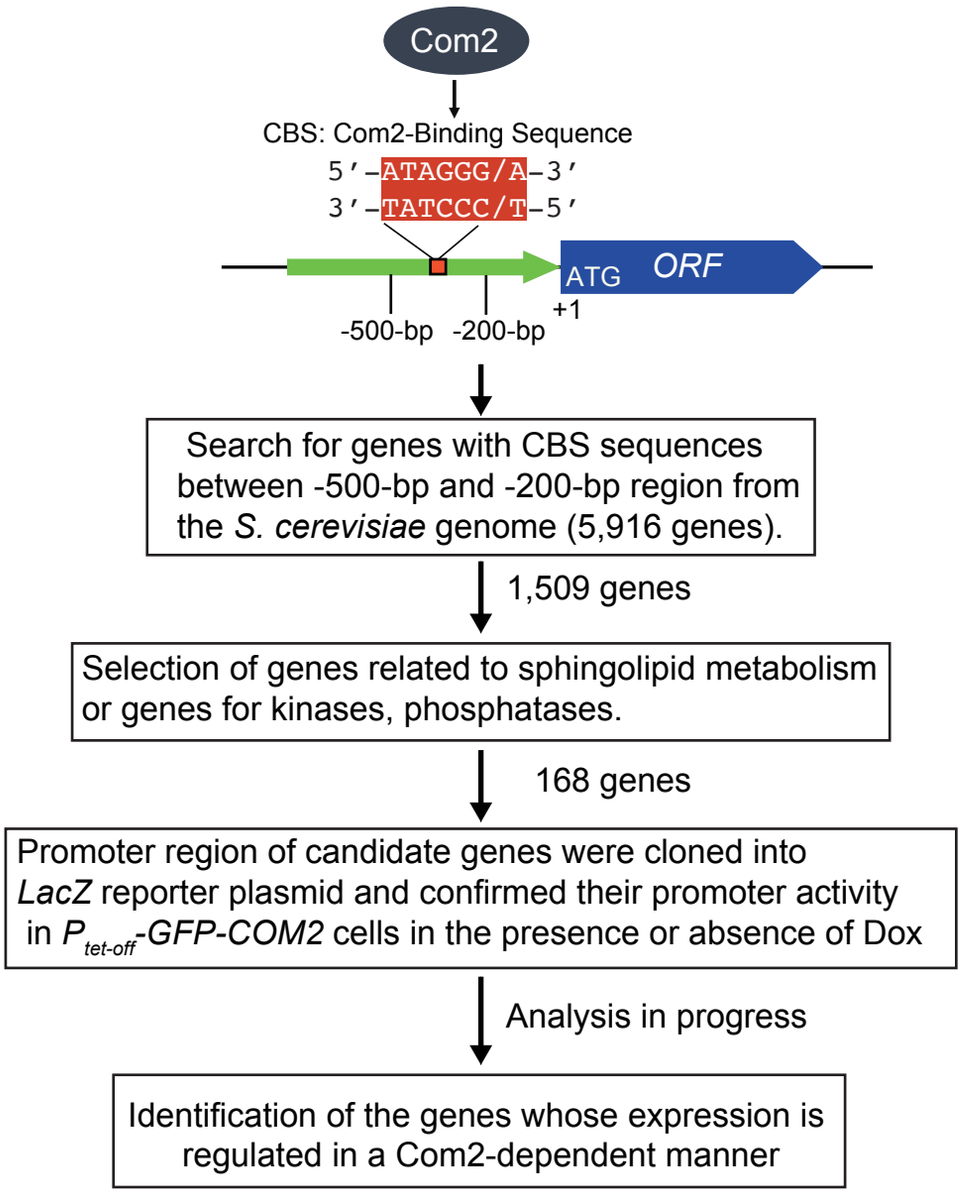

Figure 4-figure supplement 1

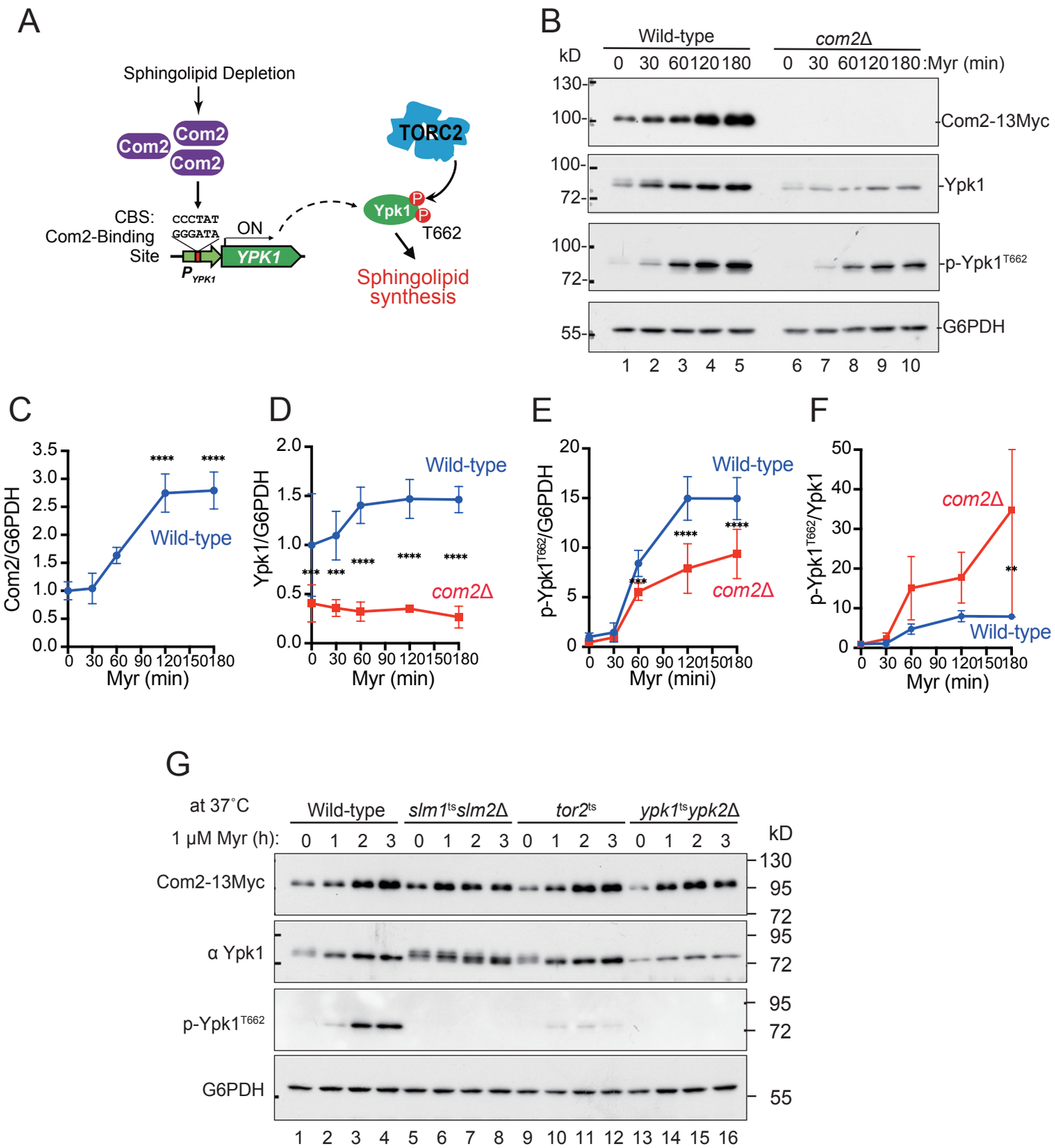
A
Sphingolipid Depletion
Com2
Com2
Com2
CBS:
Com2-Binding
Site
CCCTAT
GGGATA
ON
YPK1
P YPK1
TORC2
Ypk1
P
P
T662
Sphingolipid
synthesis
B
kD
Wild-type
com2Δ
0 30 60120180 0 30 60120180 :Myr (min)
130-
100-
Com2-13Myc
100-
72-
Ypk1
100-
72-
p-Ypk1T662
55-
G6PDH
1 2 3 4 5 6 7 8 9 10
C
Com2/G6PDH
Wild-type
Myr (min)
D
Ypk1/G6PDH
Wild-type
com2Δ
Myr (min)
E
p-Ypk1T662/G6PDH
Wild-type
com2Δ
Myr (mini)
F
p-Ypk1T662/Ypk1
com2Δ
Wild-type
Myr (min)
G
at 37˚C
Wild-type
slm1tsslm2Δ
tor2ts
ypk1tsypk2Δ
1 μM Myr (h):
0 1 2 3 0 1 2 3 0 1 2 3 0 1 2 3
kD
Com2-13Myc
130
95
72
α Ypk1
95
72
p-Ypk1T662
95
72
G6PDH
55
1 2 3 4 5 6 7 8 9 10 11 12 13 14 15 16

Figure 3

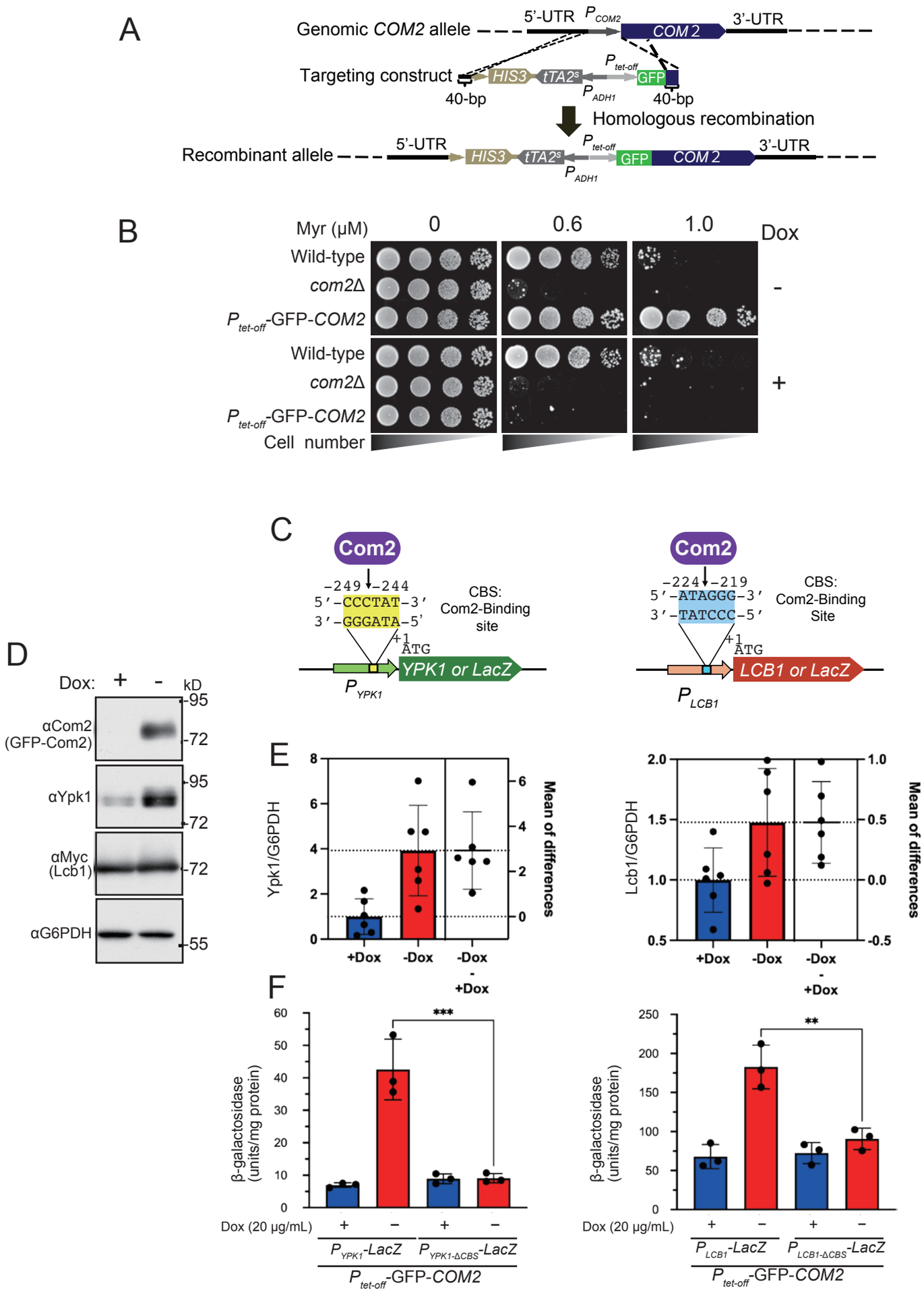
A
Genomic COM2 allele
5'-UTR
P COM2
COM 2
3'-UTR
Targeting construct
HIS3
tTA2s
P tet-off
GFP
40-bp
P ADH1
40-bp
Homologous recombination
Recombinant allele
5'-UTR
HIS3
tTA2s
P tet-off
GFP
COM 2
3'-UTR
P ADH1
B
Myr (μM)
0
0.6
1.0
Dox
Wild-type
com2Δ
P tet-off-GFP-COM2
-
Wild-type
com2Δ
P tet-off-GFP-COM2
+
Cell number
C
Com2
-249 -244
5'-CCCTAT-3'
3'-GGGATA-5'
CBS:
Com2-Binding
site
+1
ATG
YPK1 or LacZ
P YPK1
Com2
-224 -219
5'-ATAGGG-3'
3'-TATCCC-5'
CBS:
Com2-Binding
Site
+1
ATG
LCB1 or LacZ
P LCB1
D
Dox: + -
kD
αCom2
(GFP-Com2)
95
72
αYpk1
95
72
αMyc
(Lcb1)
72
αG6PDH
55
E
Ypk1/G6PDH
Mean of differences
+Dox
-Dox
-Dox
-
+Dox
Lcb1/G6PDH
Mean of differences
+Dox
-Dox
-Dox
-
+Dox
F
β-galactosidase
(units/mg protein)
***
Dox (20 μg/mL)
+
−
+
−
P YPK1-LacZ
P YPK1-ΔCBS-LacZ
P tet-off-GFP-COM2
β-galactosidase
(units/mg protein)
**
Dox (20 μg/mL)
+
−
+
−
P LCB1-LacZ
P LCB1-ΔCBS-LacZ
P tet-off-GFP-COM2

Figure 4

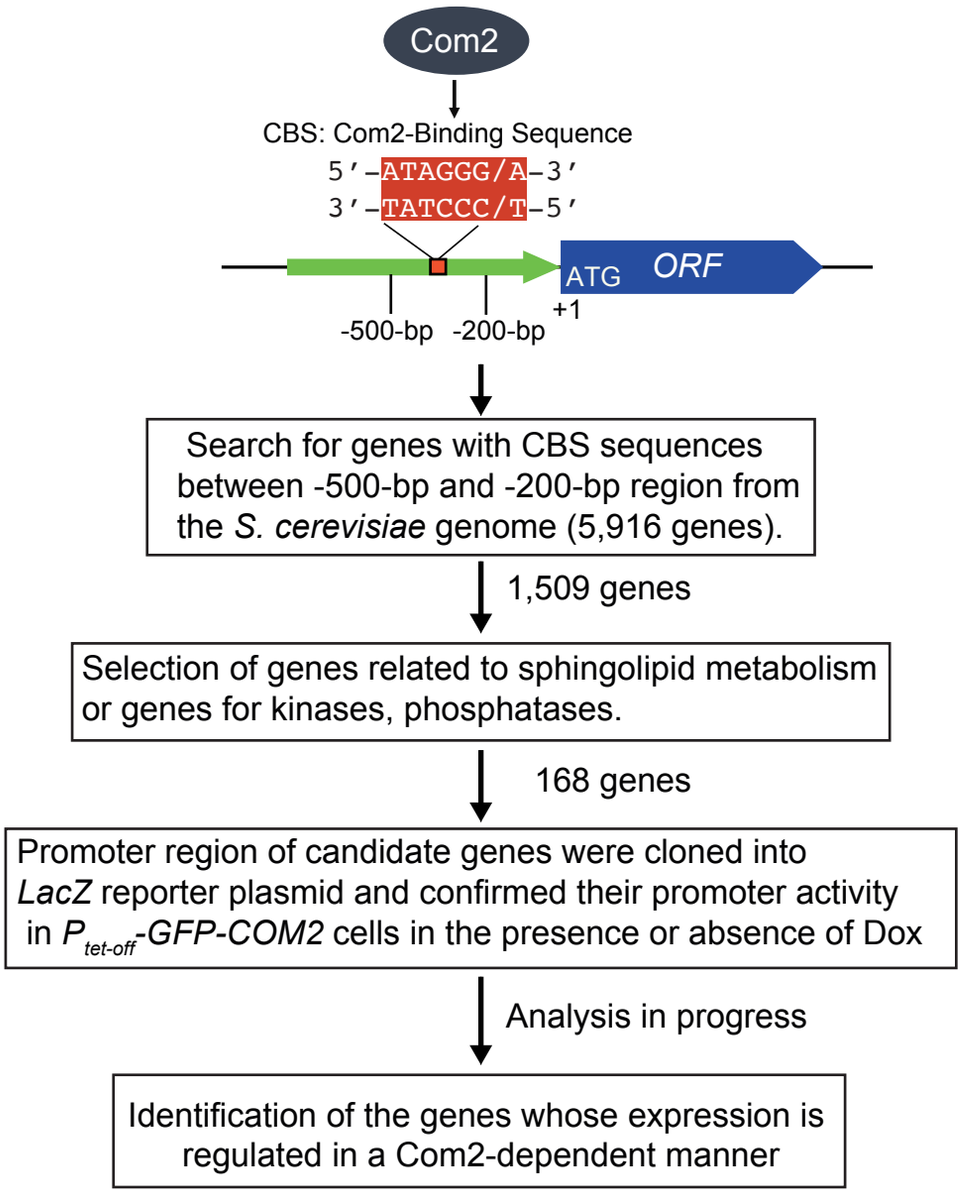

Figure 4-figure supplement 1

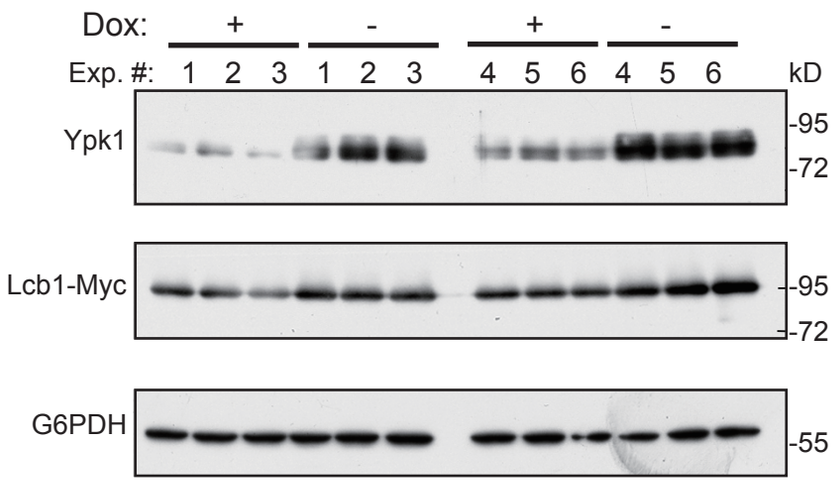

Figure 4-figure supplement 2

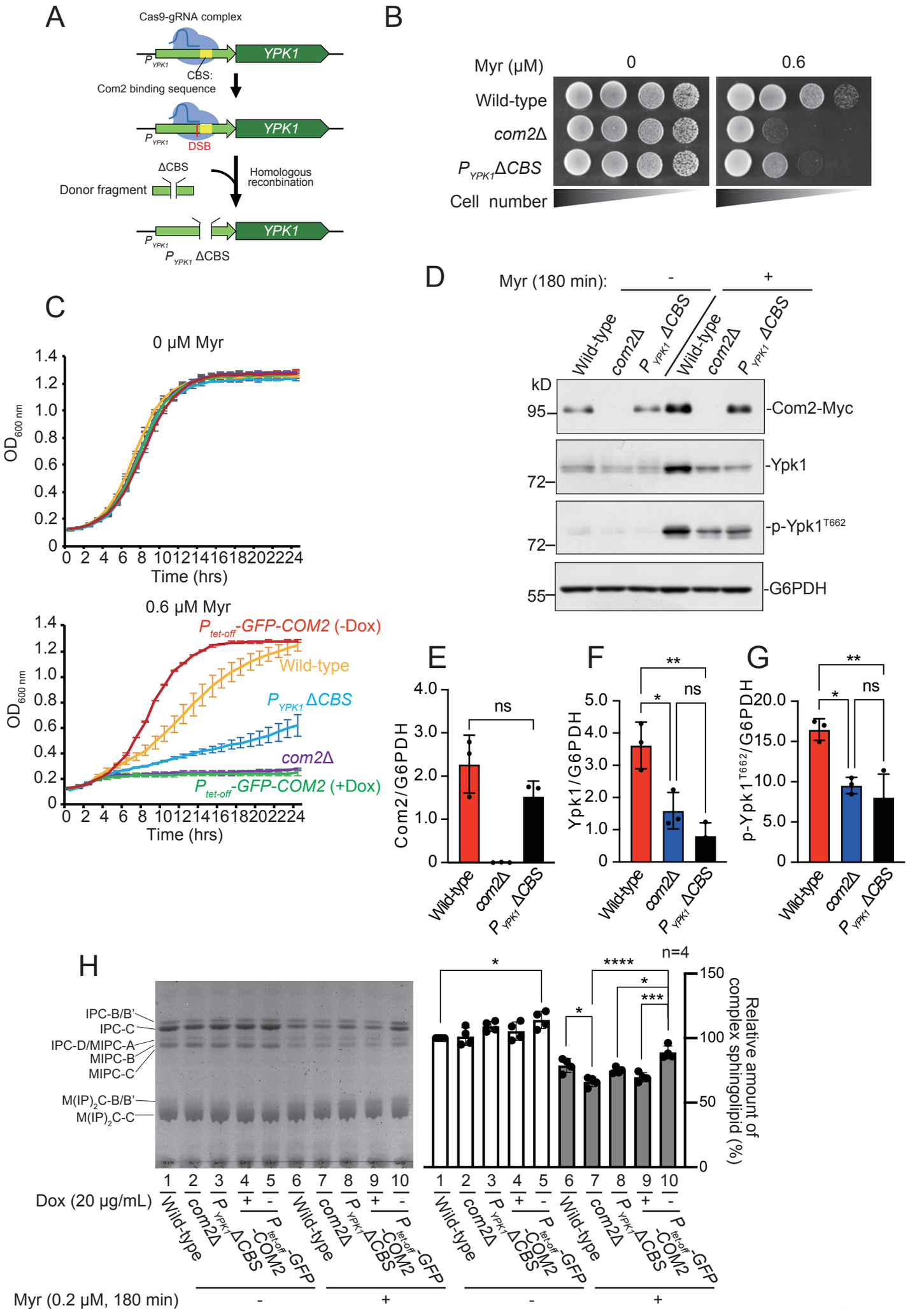
A
Cas9-gRNA complex
YPK1
CBS:
Com2 binding sequence
DSB
ΔCBS
Donor fragment
Homologous recombination
B
Myr (μM)
0
0.6
Wild-type
com2Δ
Cell number
C
0 μM Myr
0.6 μM Myr
Time (hrs)
-GFP-COM2 (-Dox)
Wild-type
ΔCBS
com2Δ
-GFP-COM2 (+Dox)
D
Myr (180 min):
-
+
kD
95
72
55
-Com2-Myc
-Ypk1
-p-Ypk1T662
-G6PDH
E
F
G
ns
Com2/G6PDH
Ypk1/G6PDH
p-Ypk1T662/G6PDH
H
IPC-B/B'
IPC-C
IPC-D/MIPC-A
MIPC-B
MIPC-C
M(IP)2C-B/B'
M(IP)2C-C
n=4
Relative amount of complex sphingolipid (%)
Dox (20 μg/mL)
Myr (0.2 μM, 180 min)

Figure 5

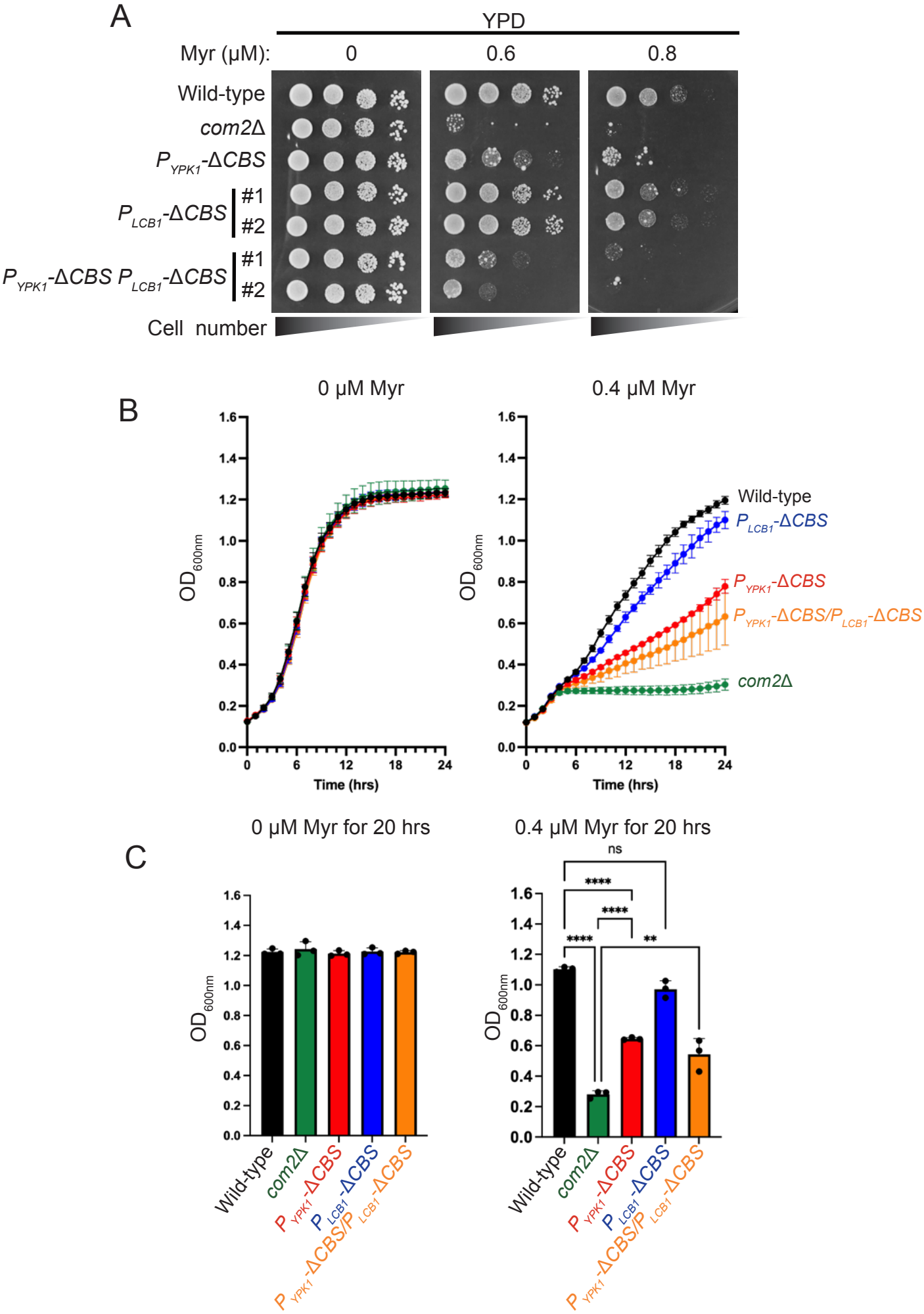

Figure 5-figure supplement

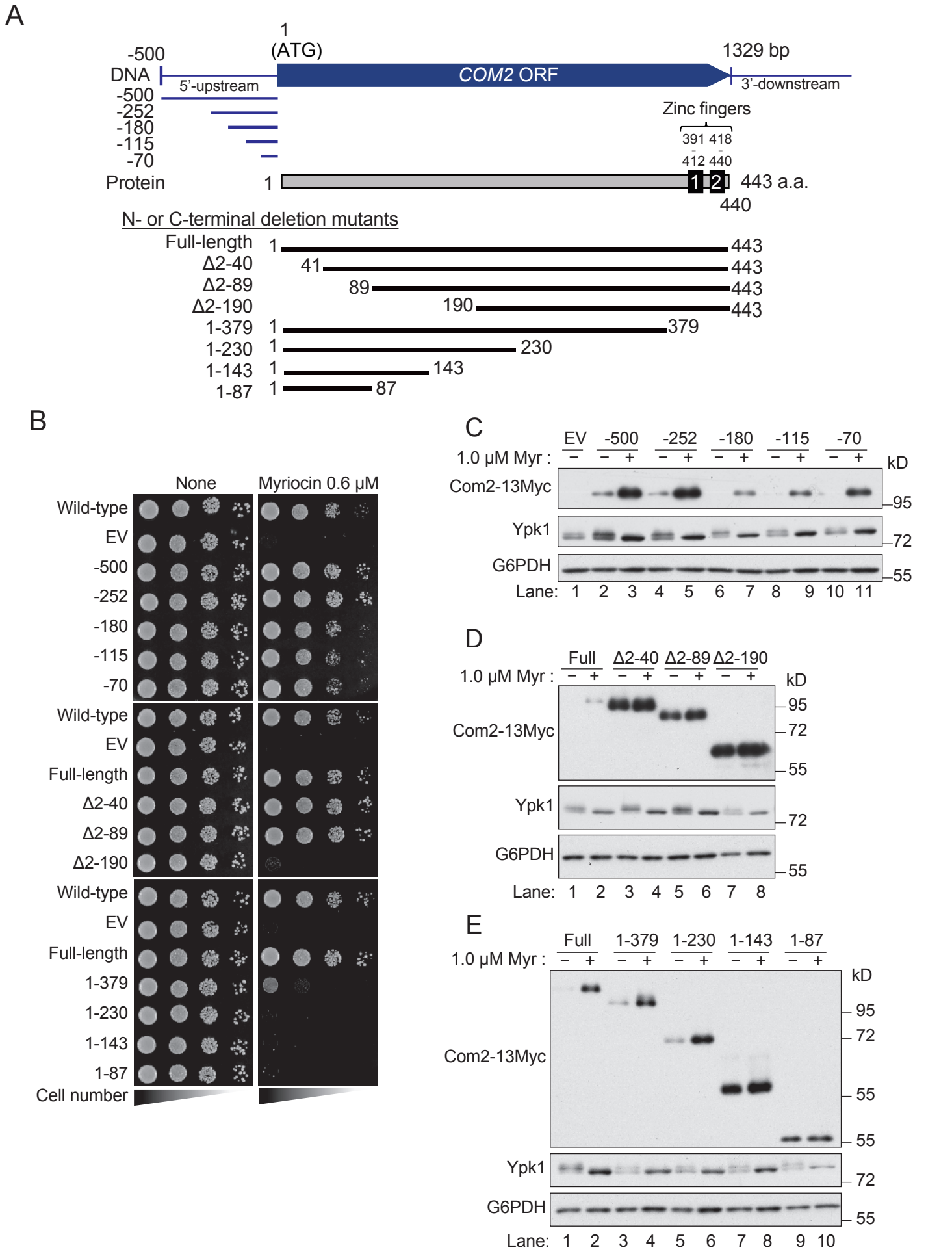
A
1
(ATG)
-500
DNA
5'-upstream
COM2 ORF
1329 bp
3'-downstream
-500
-252
-180
-115
-70
Zinc fingers
391 418
412 440
Protein
1
1 2
443 a.a.
440
N- or C-terminal deletion mutants
Full-length 1 443
Δ2-40 41 443
Δ2-89 89 443
Δ2-190 190 443
1-379 1 379
1-230 1 230
1-143 1 143
1-87 1 87
B
None
Myriocin 0.6 μM
Wild-type
EV
-500
-252
-180
-115
-70
Wild-type
EV
Full-length
Δ2-40
Δ2-89
Δ2-190
Wild-type
EV
Full-length
1-379
1-230
1-143
1-87
Cell number
C
EV -500 -252 -180 -115 -70
1.0 μM Myr : − − + − + − + − + − +
kD
Com2-13Myc
95
Ypk1
72
G6PDH
55
Lane: 1 2 3 4 5 6 7 8 9 10 11
D
Full Δ2-40 Δ2-89 Δ2-190
1.0 μM Myr : − + − + − + − +
kD
Com2-13Myc
95
72
55
Ypk1
72
G6PDH
55
Lane: 1 2 3 4 5 6 7 8
E
Full 1-379 1-230 1-143 1-87
1.0 μM Myr : − + − + − + − + − +
kD
Com2-13Myc
95
72
55
55
Ypk1
72
G6PDH
55
Lane: 1 2 3 4 5 6 7 8 9 10

Figure 6

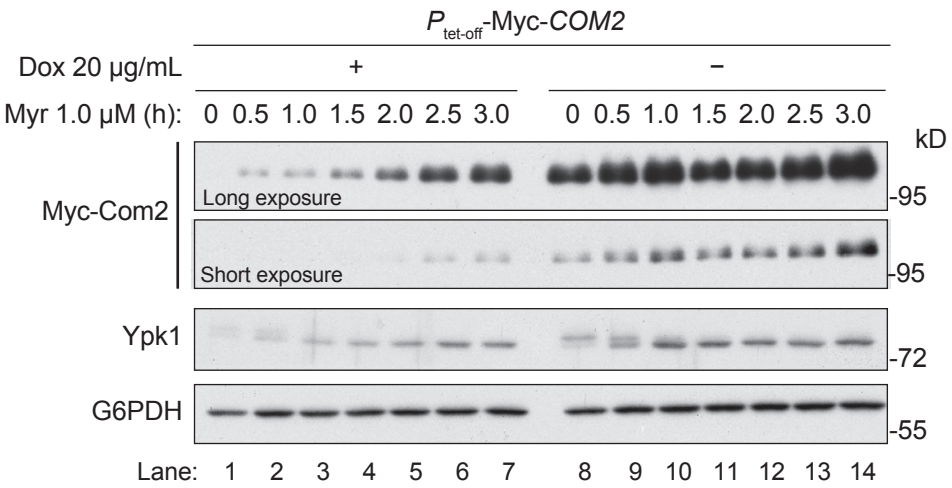

Figure 6-figure supplement

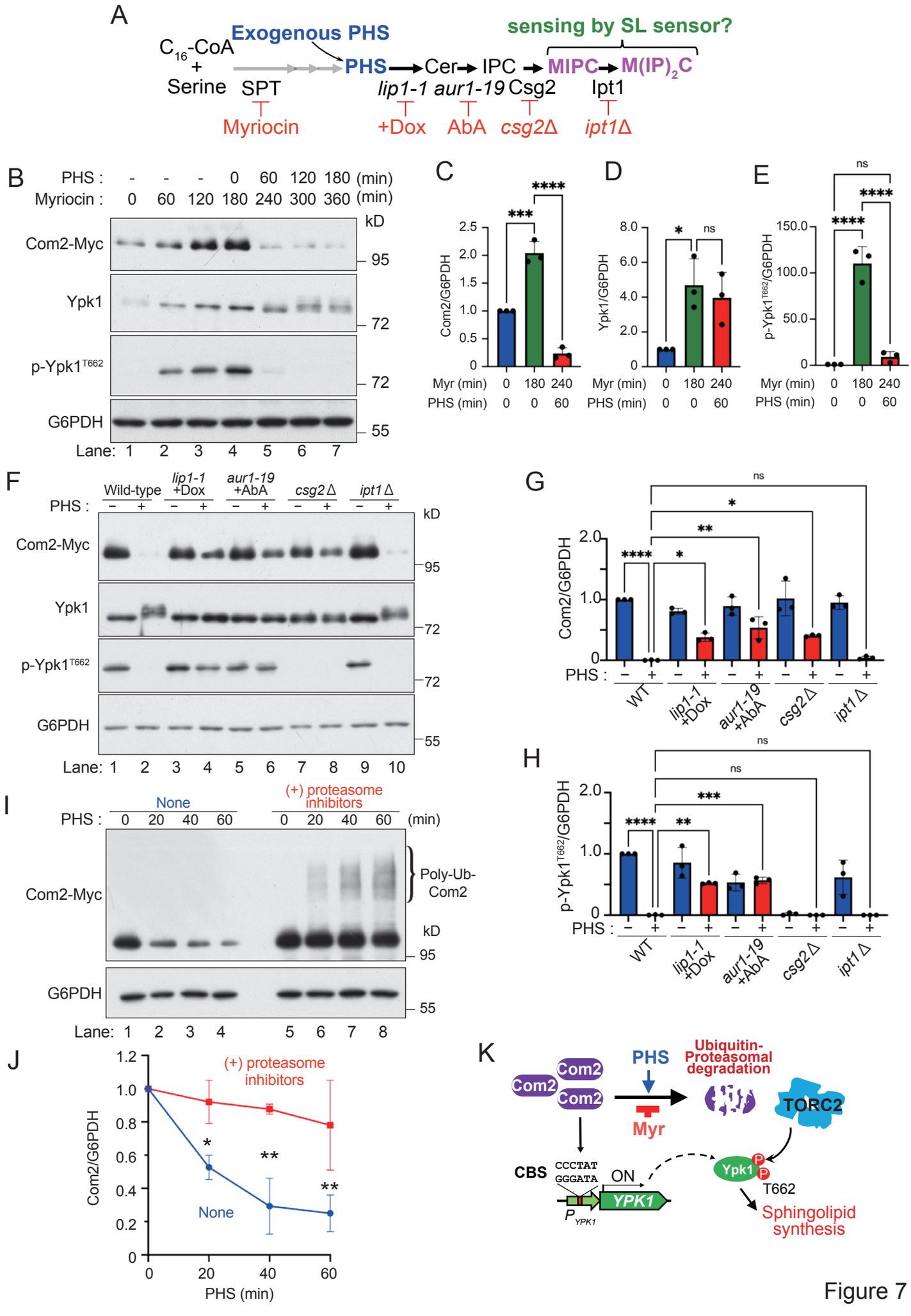
A
Exogenous PHS
sensing by SL sensor?
C16-CoA + Serine
SPT
PHS
Cer
IPC
MIPC
M(IP)2C
lip1-1 aur1-19 Csg2
Ipt1
Myriocin
+Dox
AbA
csg2Δ
ipt1Δ
B
PHS : - - - 0 60 120 180 (min)
Myriocin : 0 60 120 180 240 300 360 (min)
kD
Com2-Myc
Ypk1
p-Ypk1T662
G6PDH
95
72
72
55
Lane: 1 2 3 4 5 6 7
C
Com2/G6PDH
Myr (min) 0 180 240
PHS (min) 0 0 60
D
Ypk1/G6PDH
E
p-Ypk1T662/G6PDH
ns
F
Wild-type
lip1-1 +Dox
aur1-19 +AbA
csg2Δ
ipt1Δ
PHS : – + – + – + – + – +
Lane: 1 2 3 4 5 6 7 8 9 10
G
Com2/G6PDH
WT
lip1-1 +Dox
aur1-19 +AbA
csg2Δ
ipt1Δ
H
p-Ypk1T662/G6PDH
I
None
(+) proteasome inhibitors
PHS : 0 20 40 60 0 20 40 60 (min)
Poly-Ub-Com2
Lane: 1 2 3 4 5 6 7 8
J
(+) proteasome inhibitors
None
Com2/G6PDH
PHS (min)
K
Com2
PHS
Ubiquitin-Proteasomal degradation
Myr
TORC2
CBS
CCCTAT
GGGATA
ON
YPK1
PYPK1
Ypk1
T662
Sphingolipid synthesis

Figure 7

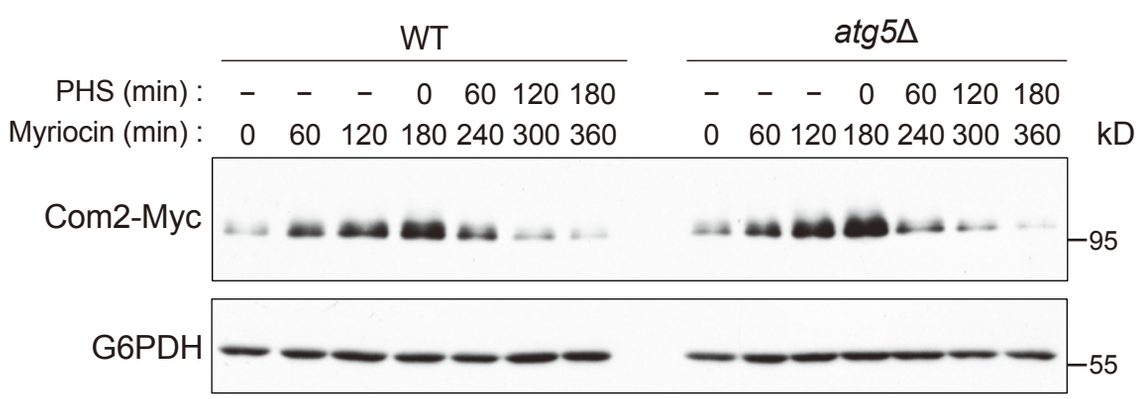

Figure 7-figure supplement

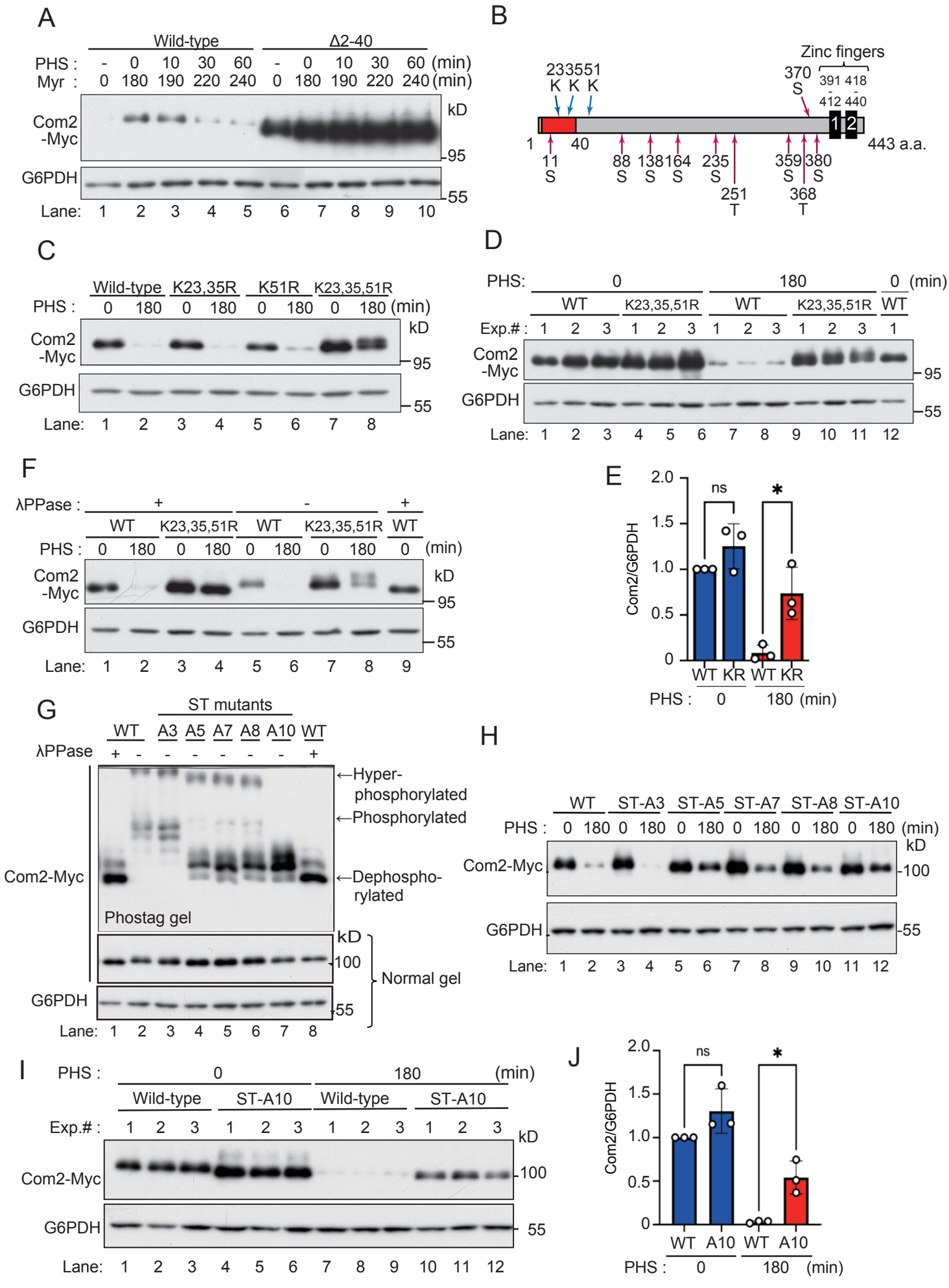
A
Wild-type
Δ2-40
PHS : - 0 10 30 60 - 0 10 30 60 (min)
Myr : 0 180 190 220 240 0 180 190 220 240 (min)
Com2 -Myc
G6PDH
kD
95
55
Lane: 1 2 3 4 5 6 7 8 9 10
B
Zinc fingers
233551
K K K
370
S
391 418
412 440
1 2
1
40
443 a.a.
11 S
88 S
138 S
164 S
235 S
251 T
359 S
380 S
368 T
C
Wild-type K23,35R K51R K23,35,51R
PHS : 0 180 0 180 0 180 0 180 (min)
Com2 -Myc
G6PDH
kD
95
55
Lane: 1 2 3 4 5 6 7 8
D
PHS: 0 180 0 (min)
WT K23,35,51R WT K23,35,51R WT
Exp.# : 1 2 3 1 2 3 1 2 3 1 2 3 1
Com2 -Myc
G6PDH
95
55
Lane: 1 2 3 4 5 6 7 8 9 10 11 12
F
λPPase : + - +
WT K23,35,51R WT K23,35,51R WT
PHS : 0 180 0 180 0 180 0 180 0 (min)
Com2 -Myc
G6PDH
kD
95
55
Lane: 1 2 3 4 5 6 7 8 9
E
Com2/G6PDH
2.0
1.5
1.0
0.5
0
ns
*
WT KR WT KR
PHS : 0 180 (min)
G
ST mutants
WT A3 A5 A7 A8 A10 WT
λPPase + - - - - - - +
Com2-Myc
Phostag gel
←Hyper-phosphorylated
←Phosphorylated
←Dephospho-rylated
kD
100
Normal gel
G6PDH
55
Lane: 1 2 3 4 5 6 7 8
H
WT ST-A3 ST-A5 ST-A7 ST-A8 ST-A10
PHS : 0 180 0 180 0 180 0 180 0 180 0 180 (min)
kD
Com2-Myc
100
G6PDH
55
Lane: 1 2 3 4 5 6 7 8 9 10 11 12
I
PHS : 0 180 (min)
Wild-type ST-A10 Wild-type ST-A10
Exp.# : 1 2 3 1 2 3 1 2 3 1 2 3
kD
Com2-Myc
100
G6PDH
55
Lane: 1 2 3 4 5 6 7 8 9 10 11 12
J
Com2/G6PDH
2.0
1.5
1.0
0.5
0
ns
*
WT A10 WT A10
PHS : 0 180 (min)

Figure 8

A

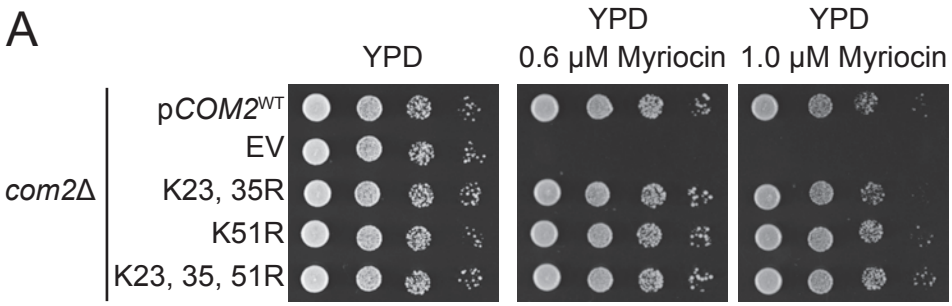

B

position	Sequence	SGD*	Ypk1**	SGK1***	SGK3***	SGK***	AGC***	ST-A3	ST-A5	ST-A7	ST-A8	ST-A10
11S	YPLQRFE**S**NDTVFSY	+										+
88S	NQLERRL**S**ISDYRTE	+			+		+		+	+	+	+
138S	ESDVLMV**S**DDELEVN	+										+
164S	DGLNRIS**S**TNNLKNL	+			+				+	+	+	+
235S	PIQTENS**S**SQKMFKN			+		+				+	+	+
251T	FFRSRKS**T**LIKSLPL		+		+	+	+	+	+	+	+	+
359S	SVQSSSS**S**HGLVVRK					+				+	+	+
368T	GLVVRKK**T**GSMQKTR			+			+				+	+
370S	VVRKKTG**S**MQKTRGR		+	+	+	+	+	+	+	+	+	+
380S	KTRGRKP**S**LIPDASK	+	+			+	+	+	+	+	+	+

*SGD: https://www.yeastgenome.org/locus/S000000932/protein

**Muri et al., eLife: https://elifesciences.org/articles/03779

***GPS web server : http://gps.biocuckoo.org/online.php

C

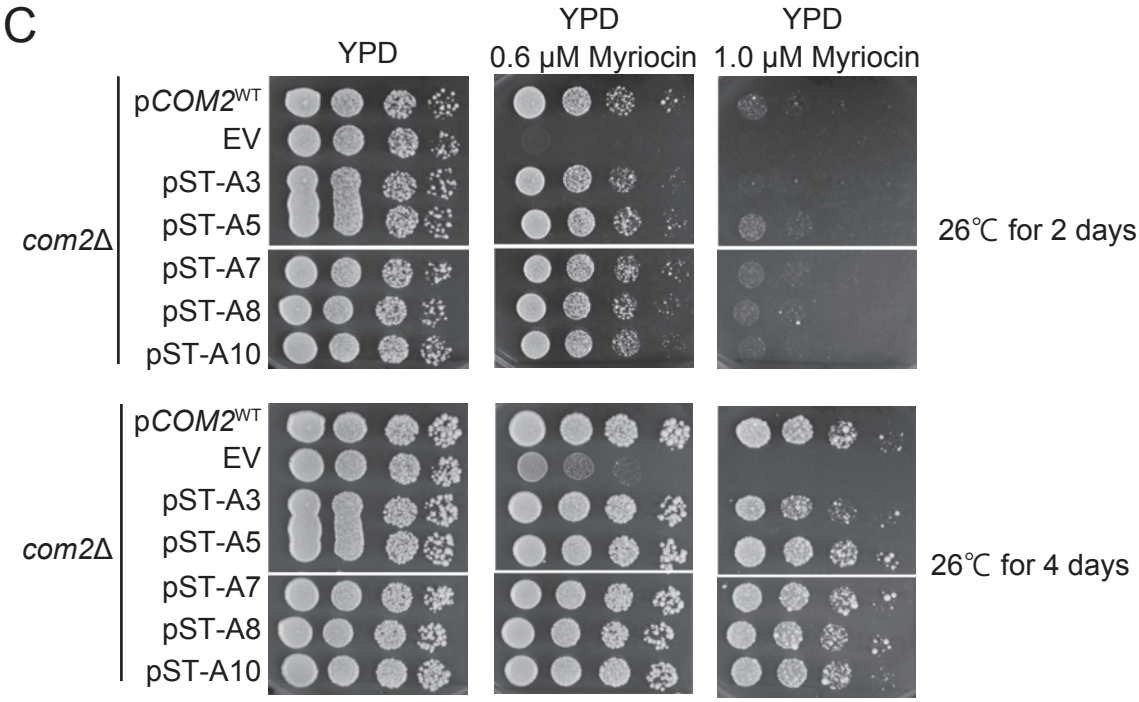

Figure 8-figure supplement

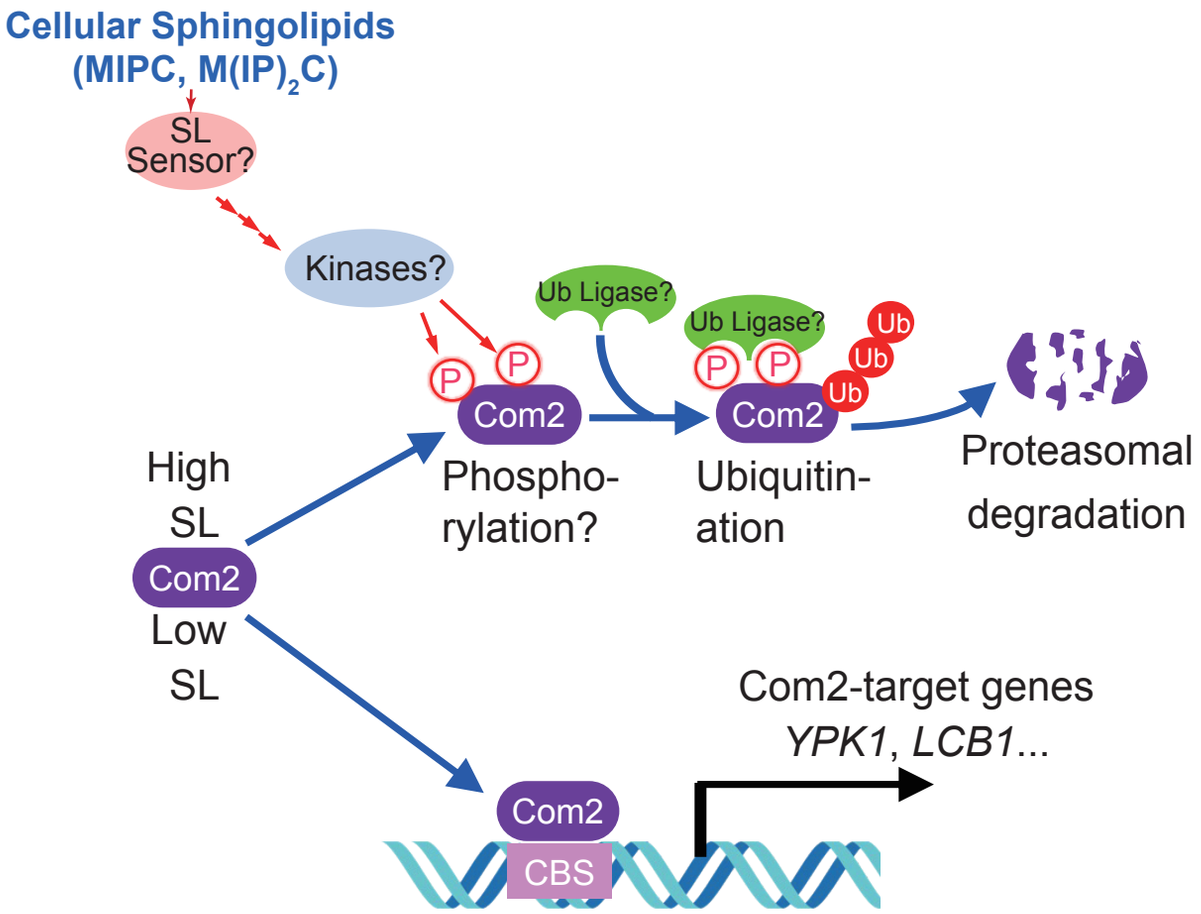
Cellular Sphingolipids
(MIPC, M(IP)2C)
SL
Sensor?
Kinases?
Ub Ligase?
Ub Ligase?
P
P
P
P
Ub
Ub
Ub
Com2
Com2
High
SL
Com2
Low
SL
Phospho-
rylation?
Ubiquitin-
ation
Proteasomal
degradation
Com2-target genes
YPK1, LCB1...
Com2
CBS

Figure 9